**Atmospheric
Chemistry
and Physics**

On the diurnal cycle of urban aerosols, black carbon and the occurrence of new particle formation events in springtime São Paulo, Brazil

J. Backman[1], L. V. Rizzo[2], J. Hakala[1], T. Nieminen[1], H. E. Manninen[1], F. Morais[3], P. P. Aalto[1], E. Siivola[1], S. Carbone[4], R. Hillamo[4], P. Artaxo[3], A. Virkkula[1,4], T. Petäjä[1], and M. Kulmala[1]

[1]Division of Atmospheric Sciences, Department of Physics, University of Helsinki, Helsinki, Finland
[2]Department of Earth and Exact Sciences, Federal University of São Paulo, São Paulo, Brazil
[3]Institute of Physics, University of São Paulo, São Paulo, Brazil
[4]Finnish Meteorological Institute, Helsinki, Finland

Correspondence to: J. Backman (john.backman@helsinki.fi)

Abstract. Large conurbations are a significant source of the anthropogenic pollution and demographic differences between cities that result in a different pollution burden. The metropolitan area of São Paulo (MASP, population 20 million) accounts for one fifth of the Brazilian vehicular fleet. A feature of MASP is the amount of ethanol used by the vehicular fleet, known to exacerbate air quality. The study describes the diurnal behaviour of the submicron aerosol and relies on total particle number concentration, particle number size distribution, light scattering and light absorption measurements. Modelled planetary boundary layer (PBL) depth and air mass movement data were used to aid the interpretation. During morning rush-hour, stagnant air and a shallow PBL height favour the accumulation of aerosol pollution. During clear-sky conditions, there was a wind shift towards the edge of the city indicating a heat island effect with implications on particulate pollution levels at the site. The median total particle number concentration for the submicron aerosol typically varied in the range 1.6×10^4–3.2×10^4 cm^{-3} frequently exceeding 4×10^4 cm^{-3} during the day. During weekdays, nucleation-mode particles are responsible for most of the particles by numbers. The highest concentrations of total particle number concentrations and black carbon (BC) were observed on Fridays. Median diurnal values for light absorption and light scattering (at 637 nm wavelength) varied in the range 12–33 Mm^{-1} and 21–64 Mm^{-1}, respectively. The former one is equal to 1.8–5.0 µg m^{-3} of BC. The growth of

the PBL, from the morning rush-hour until noon, is consistent with the diurnal cycle of BC mass concentrations. Weekday hourly median single-scattering albedo (ω_0) varied in the range 0.59–0.76. Overall, this suggests a top of atmosphere (TOA) warming effect. However, considering the low surface reflectance of urban areas, for the given range of ω_0, the TOA radiative forcing can be either positive or negative for the sources within the MASP. On the average, weekend ω_0 values were 0.074 higher than during weekdays. During 11 % of the days, new particle formation (NPF) events occurred. The analysed events growth rates ranged between 9 and 25 nm h^{-1}. Sulphuric acid proxy concentrations calculated for the site were less than 5 % of the concentration needed to explain the observed growth. Thus, other vapours are likely contributors to the observed growth.

1 Introduction

Atmospheric aerosols affect human health and well-being (Davidson et al., 2005; Nel, 2005). They affect visibility and the radiative forcing. The radiative forcing can either be direct by scattering and absorbing solar irradiation (e.g. Haywood and Boucher, 2000; Ramanathan et al., 2001; IPCC, 2007; Ramanathan and Carmichael, 2008) or indirect by acting as a cloud condensation nuclei (CCN, Clarke and Kapustin, 2010; Lohmann and Feichter, 2005; Pöschl et al.,

2010). The potential of the aerosol particles to alter these depends on their number concentration, size and chemical composition (Haywood and Boucher, 2000). Once emitted, pollutants in the gas and particulate phases are subject to atmospheric processing. They can either be emitted directly into the atmosphere as primary aerosol particles or be formed there as secondary aerosol particles.

Among the primary aerosol particles, significant attention has been put onto light absorbing aerosols, emitted as a result of incomplete combustion processes, profuse in urban areas. During the last two decades studies have shown the climatic effects of light absorbing aerosols (e.g. Haywood and Shine, 1995; Andreae, 2001; Jacobson, 2001; Ramanathan and Carmichael, 2008). Bond and Bergstrom (2006) recommend the term light absorbing carbon (LAC) for light-absorbing carbonaceous aerosols, although black carbon (BC) is still the most widely used therm. In this paper, we will use the term BC, since it was the output of the instrument we used. Atmospheric BC, a potent radiative forcer, also possess the ability to change the temperature profile of the atmosphere by adding energy to the atmosphere and reducing it at the surface (e.g. Ramanathan and Carmichael, 2008).

Secondary aerosols are more complex by nature (e.g. Hallquist et al., 2009; Jimenez et al., 2009; Kroll and Seinfeld, 2008; Rudich et al., 2007). Secondary aerosol gas-particle conversion processes include inorganic species such as sulphate, nitrate, and ammonium (e.g. Zhang et al., 2000). Organic species are also substantial contributors to the submicron particulate mass (Jimenez et al., 2009). A gain in secondary aerosol mass will affect the optical properties of the aerosol. The sheer number of organics in the atmosphere, and the plethora of intermediate products is an immense challenge for the accurately prediction SOA formation (Hallquist et al., 2009; Rudich et al., 2007). The vapour pressure of organics, and thus their SOA-formation potential, depends on their polarity and size. The addition of common oxygen containing functional groups, e.g. the hydroxyl (OH) radical, the hydroperoxyl (HO_2) radical, and the nitrate (NO_3) radical will reduce the vapour pressure of organics significantly (Kroll and Seinfeld 2008), yielding less volatile and more water soluble products in the process (Hallquist et al., 2009). Oxidation reactions through which VOCs evolve are primarily initiated by OH radical, NO_3 radical, and ozone (O_3, Hallquist et al., 2009; Kroll and Seinfeld, 2008). The products that follow can subsequently end up in the condensed phase, where they are still susceptible to processes in either phase, and will further evolve through heterogeneous and multiphase reactions over many generations (Kroll and Seinfeld, 2008). Hence, SOA yields from even a single precursor are not a stoichiometric quantity but increases with organic-particulate loading (Hallquist et al., 2009; Kroll and Seinfeld, 2008). Given the multitude of intermediate and interacting reactions in multiple phases we focus the discussion

on the initiating oxidants from an ethanol combustion point of view, and thus stay within the scope of the study.

Large conurbations are a significant source of primary and secondary aerosol particles and trace gases, with potential effects on the hydrological cycle (Lohmann and Feichter, 2005) and climate patterns (IPCC, 2007). We know from previous studies that megacities differ from each other in terms of trace-gas levels, particle emission, and ambient air quality (Gurjar et al., 2008; Laakso et al., 2006). Unlike coarse-mode particles, fine-mode particles (i.e. submicron) are mostly of anthropogenic origin consisting commonly of sulphates, nitrates, organics, and BC. Sulphates, nitrates and organics scatter light, while BC also absorbs light. Together, these fine-mode particles make up the urban haze, characteristic for polluted areas.

Previous studies (e.g. Kittelson et al., 2004; Zhu et al., 2002) have shown vehicular exhaust to be a significant source of nucleation-mode particles in urban areas. Nucleation-mode particles can also be produced through new particle formation (NPF). NPF, and the growth of these newly formed particles, depends on the concentration of gaseous vapours, the production of nanometer-size clusters and the pre-existing aerosol population (Kerminen et al., 2001; Kulmala, 2003). In the initial formation and growth, sulphuric acid is a vital contributor (Sipilä et al., 2010). The presence of sulphuric acid has also been shown to catalyse heterogeneous reactions of aldehyde functional groups and yield additional aerosol mass (Jang and Kamens, 2001). Moreover, sulphuric acid concentrations can usually explain only a fraction of the observed growth rate (Kulmala et al., 2004).

The metropolitan area of São Paulo (MASP, population 20 million) is the world's seventh largest urban agglomerate with a fleet of 8.4 million registered vehicles. By numbers, this is one fifth of the Brazilian fleet (CETESB, 2007). To date, size distribution measurements within the MASP are scarce and short. Previous studies have shown elevated concentrations of trace gases associated with ethanol-based fuels in São Paulo (Colon et al., 2001; Nguyen et al., 2001). In general, this is characteristic of MASP since estimates suggest that 55 % of the vehicular fuel consumption by volume is bioethanol (CETESB, 2007). There are uncertainties associated with the use of oxygenated fuels on the implications on air quality, climate, and human health (Farrell, 2006; Gaffney and Marley, 2009; Jacobson, 2007). Bioethanol in flexi-fuel vehicles is known to reduce NO_x emissions, but increase aldehyde emissions (Graham et al., 2008). During combustion, ethanol (CH_3CH_2OH) can crack to form mainly acetaldehyde CH_3CHO (Gaffney and Marley, 2009) and some formaldehyde HCHO. Acetaldehyde is also formed when ethanol reacts with the OH radical (95 % of the time, Atkinson, 2000). Aldehydes provide pathways which produce photochemical smog (Haagen-Smit, 1952; Tanner et al., 1988; Atkinson, 2000).

Once pollutants are airborne, they are subject to boundary layer evolution and prevailing meteorological conditions.

Both the traffic-related emissions and the meteorological conditions have clear diurnal cycles. One of the goals of this paper was to study the main factors governing the diurnal cycles of the submicron aerosol properties in São Paulo. Another goal is to compare the MASP aerosol with results obtained from other urban areas to find out whether the fuel used has an effect on the aerosol properties tracked in the study.

In this paper, we analyse the diurnal cycle of submicron aerosol in terms of particles number concentration, their size distribution, optical properties, and BC concentrations associated with traffic. Thus, weekdays and weekends were treated separately, since there was more traffic during weekdays. We will describe how meteorological conditions and their diurnal cycle affect the observations. Secondary aerosol formation affecting the measurements, although not backed up by direct chemical composition data, is addressed through the optical properties of the aerosol. Furthermore, the study reports a lower limit for the sulphuric acid (H_2SO_4) concentrations required for the observed NPF growth and how they compare to a sulphuric acid proxy based on trace-gas data. This allows for an estimate on the contribution to growth by other condensable vapours in addition to H_2SO_4.

2 Methods and instrumentation

2.1 The campaign measurement site

The site is located roughly 10 km from the centre of São Paulo city, at the western edge of the most densely populated area. Vast suburban residential areas surround the city centre, populated by 20 million people. This makes São Paulo the world's 7th largest city. The city locates on a plateau 760 m above sea level (a.s.l.) surrounded by hills rising as high as 1200 m a.s.l. To the southeast, about 55 km away, is the Atlantic Ocean. Adjacent to the Atlantic Ocean there is a 15 km wide costal area before the plateau on which São Paulo situates. The steep slope of Serra do Mar inclines 700 m within 3 km. The climate is subtropical with dry winters and wet summers (Oliveira et al., 2003). The measurements were made at the Armando Salles de Oliveira campus area of USP (Fig. 1). The campus area is a vast park, totalling an area of 7.4 km^2, making the site ideal for tracking ambient aerosols, without strong local sources. At the campus area buildings are scarce. Thus, air masses arriving at the station should be well mixed and make the measurements representative of the ambient pollution burden of the city.

A temperature controlled room on the roof of a four-story building housed the measurement equipment. Two equivalent vertical sampling lines with $PM_{2.5}$ inlets mounted 0.5 m above the roof provided sample air to the instruments. Excess flow arrangements ensured the total flow in the sampling line to be 16.7 lpm. The sampling lines to the instruments were 3/8 inch stainless steel tubing with an inner di-
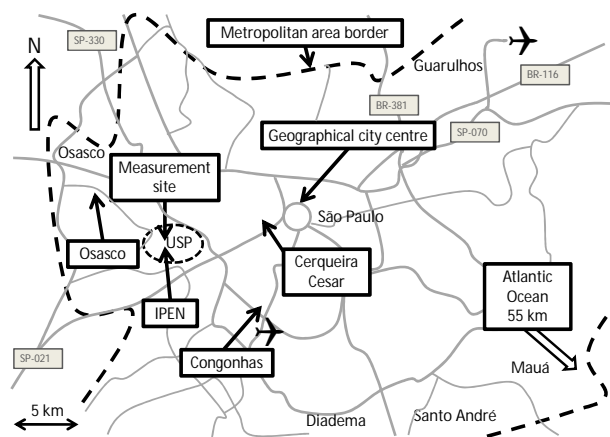
Fig. 1. Map of the metropolitan area of São Paulo. The measurement site is west of the geographical city centre. The metropolitan area of São Paulo is inhabited by 20 million people.

ameter of 1/4 inch from the inlet to the instruments and 1.8 m in length. Aerosol optical instruments were sampling through one sampling line. Total particle number concentrations were sampling through the other sampling line in parallel with the size distribution measurements. Total particle number concentrations were measured with a condensation particle counter (CPC, Model 3022, TSI Inc., St. Paul, MN, USA) and number size distributions with a differential mobility particle sizer (DMPS, Knutson and Whitby, 1975). A Neutral cluster and Air Ion Spectrometer (NAIS, Kulmala and Tammet, 2007; Manninen et al. 2009), were also used to measure size distributions, placed outside in a cabinet with a sampling line of its own. Sample air was drawn into the instrument through a 0.6 m long copper tube with a sample flow of 60 lpm. The inner diameter of the sampling line used was 33 mm. The cabinet temperature was kept above ambient to avoid condensation inside the instrument.

2.2 Supporting measurement stations

In addition to the measurements at the campaign site, we took use of meteorological and trace gas measurements from existing measurements stations. The meteorological station closest to the campaign site was 100 m away at the Institute of Astronomy, Geophysics and Atmospheric Science (IAG, Oliveira et al., 2002). The meteorological station operated by the micrometeorology group at USP provided us with temperature, pressure, precipitation, relative humidity and global irradiance data.

In addition, trace gas data provided by CETESB were used in the analysis. They maintain a network of atmospheric monitoring stations in the state of São Paulo. The closest CETESB measurement station is IPEN (Fig. 1), located 600 m to the south of the campaign site within the campus area. Both IPEN and the campaign site are in the

western part of the campus area. The IPEN station monitors O_3. The closest available station measuring sulphur dioxide (SO_2) was the Osasco monitoring station located 6 km away to the northwest (Fig. 1). It is located in the residential and to some extent commercial municipality of Osasco with relatively few high rise buildings in comparison to São Paulo. Also, commuter avenues were not within the immediate surroundings of the site, but approximately 1 km away to the north. Two other monitoring stations, Congonhas and Cerqueira Cesar, considered for the analysis were omitted due to their different surroundings in comparison to the measurement site (Gallardo et al., 2012). The Cerqueira Cesar monitoring station (7 km to the west) is more representative of street-level pollution exposure than of the ambient levels at the campaign site, because of its close location to an eight-lane avenue. Further south, 9 km to the southwest of the campaign site is the Congonhas measurement station. Heavy roadside traffic and the central airport of São Paulo (1 km away) are the dominant features of Congonhas (Gallardo et al., 2012). Therefore, we decided to use the Osasco SO_2 data in the analysis since it resembles the measurement site the most. The station is also the only one which tracks wind direction and wind speed in addition to SO_2.

2.3 Instrumentation

2.3.1 Differential mobility particle sizer (DMPS)

Submicron aerosol number size distribution and total particle number concentration was monitored with a DMPS system (Aalto et al., 2001). To minimise diffusion losses two aerosol flow arrangements were used in the same Vienna-type Differential Mobility Analyzer (DMA, Winklmayr et al., 1991) with closed sheath flow arrangements. The DMPS measured number size distributions from 6–800 nm mobility diameters. For smaller particles, a high aerosol flow of $4 \, \text{L} \, \text{min}^{-1}$ and a sheath flow of $20 \, \text{L} \, \text{min}^{-1}$ were used to measure mobility diameters from 6–280 nm. Mobility diameters from 100–800 nm were measured with an aerosol flow of $1 \, \text{L} \, \text{min}^{-1}$ and a sheath flow of $5 \, \text{L} \, \text{min}^{-1}$. These flow rates result in the same non-diffusional transfer function with a β of 1/5 as described by Zhang and Flagan (1996).

2.3.2 Neutral cluster and Air Ion Spectrometer

The deployment of a Neutral cluster and Air Ion Spectrometer (NAIS) enabled the tracking of the initial steps of NPF. The NAIS measures mobility distributions in the range 3.2–$0.0013 \, \text{cm}^2 \, \text{V}^{-1} \, \text{s}^{-1}$ and corresponds to mobility diameters in the range of 0.8–42 nm (Mirme et al., 2007). The instrument is a further development of the Air Ion Spectrometer (AIS) which only measures naturally charged particles. The ability of the NAIS to measure neutral clusters arises from the unipolar corona chargers. In the neutral-particle mode, particles are charged with corona chargers and the charging

probability is calculated using Fuchs theory (Fuchs, 1963). Before the sample enters the DMAs, some of the corona charger ions are filtered out using electrical post-filters. Mobility distributions are measured with two DMAs in parallel, one for each polarity. The central electrodes of the DMAs have a polarity opposite to the charger surrounded by 21 circular electrometers. The oppositely charged particles entering the vicinity of the DMA precipitate onto the outer walls away from the central electrode onto the electrometers. Electrometer currents are inverted to 28 different size bins taking into account experimentally determined diffusion losses and instrument noise (Mirme and Mirme, 2011). The noise of the electrometers were measured subsequently and subtracted from the measurements thus minimizing the influence of any reduction in electrometer performance. A schematic of the instrument is presented in Manninen et al. (2009).

The post-filters were manually tuned so that not all of the main charger ions are removed with the result that the instrument performance can be tracked better. Combined DMPS and NAIS number size distributions were plotted from 3–800 nm, thus discarding these charger ions. Although the NAIS and DMPS measure the same aerosol, the inversion, charging probability, and charging method differ.

2.3.3 Aerosol optical instruments

The optical properties tracked were light scattering coefficients (σ_{SP}) measured by a Nephelometer (Model 3563, TSI Inc., St. Paul, MN, USA) and light absorption coefficients (σ_{AP}) converted from black carbon (BC) mass concentrations reported by a Multi Angle Absorption Photometer (MAAP, Model 5012, Thermo Scientific, Franklin, MA, USA). The aerosol was dried with diffusion driers. The instruments were coupled in series with a flow rate of 10 lpm using the MAAP's internal pump downstream of the Nephelometer.

The Nephelometer measures light scattering coefficients at 450, 550, 700 nm wavelengths (Anderson and Ogren, 1998). At the same time, it tracks the relative humidity (RH), temperature and pressure of the sample air inside the instrument. Scattering coefficients were corrected for angular truncation error according to Anderson and Ogren (1998). Instrument calibration was done using particle-free air and carbon dioxide. Scattering coefficients measured with a RH exceeding 50 % inside the instrument were discarded, which were less than 30 % of the data set.

The BC concentrations were measured with a MAAP (Petzold et al., 2005) at the wavelength of 637 nm (Müller et al., 2011). σ_{AP} was calculated from the BC concentrations using the mass absorption cross-section (MAC) of $6.6 \, \text{m}^2 \, \text{g}^{-1}$. The relationship between σ_{AP} and BC mass concentrations is

$$\sigma_{\text{AP}} = \text{MAC} \cdot \text{BC}. \tag{1}$$

Furthermore, as suggested by Müller et al. (2011), a 5 % increase in light absorption was applied.

Measured aerosol optical properties were converted to 1000 mbar and 0 °C conditions from the temperature and pressure measured in the Nephelometer. Using Ångström exponents, light scattering was interpolated to the MAAP wavelength yielding the single-scattering albedo (ω_0) of the aerosol.

2.3.4 Instrument calibrations

Prior to deployment, the CPCs were calibrated with the aid of an electrometer (Model 3068, TSI Inc., St. Paul, MN, USA). The calibration setup was principally the same as is described in the technical paper by Agarwal and Sem (1978). Silver particles were produced by heating silver in an oven to 1000–1060 °C in a nitrogen atmosphere.

The calibration setup was used to determine the particle number concentrations and cut-off diameter of the CPCs against the reference electrometer in the single particle counting mode (10^3–10^4 cm^{-3}). Ideally, the particle number concentrations measured with the CPCs and the electrometer would be the same (slope 1 : 1). The slope was determined with 50 nm particles, well above the cut-off diameter of the CPCs. In the photometric mode, the CPCs were compared against each other onsite with 50 nm sodium chloride particles and operated side-by-side with the DMPS.

The cut-off diameters were determined both with and without aerosol driers inline. In this way, we were able to estimate the effect of diffusional losses in the driers, represented by an equivalent length of tube losses in the sampling line. The CPC (Model 3772, TSI Inc., St. Paul, MN, USA) used in the DMPS had a cut-off diameter of 6 nm. With the NAPHION (Permapure LLC, Toms River, NJ, USA) diffusion drier in the DMPS the cut-off size was 13 nm. From these results, the equivalent length of the drier was calculated to be 13.3 m. The cut-off diameter of the TSI 3022 CPC was 5 nm. With its Topas (Topas GmbH, Dresden, Germany) diffusion drier, the cut-off was at 7 nm. This was calculated to be equivalent to 2.7 m of sampling line. Diffusional losses in the DMA and sampling line were compensated for during the inversion of the DMPS measurement data. The determined equivalent length of the diffusion drier of the DMPS was added to the actual sampling line length. Thus, all reported DMPS size distributions were compensated for diffusional losses throughout the system.

The high voltage supply for the DMA was calibrated between 0 and 1 kV and a similar slope was assumed for the whole range. This was verified by sampling 404 nm latex particles and changing the sheath flow of the DMA.

The sheath flow of the DMA was controlled with a mass flow meter (Series 4000, TSI Inc., St. Paul, MN, USA) with HEPA filters both upstream and downstream of the device. The aerosol flow was calibrated using a flow meter (Model DC-1, Bios Inc., Butler, NJ, USA). The slope and the offset were determined by linear regression and were fed into the DMPS software. During routine maintenance, the aerosol flows were checked.

2.4 New particle formation event analysis

New particle formation (NPF) depends on the competition between the initial growth of the nuclei and their scavenging by the pre-existing particle population (Kulmala et al., 2005). The condensation sink (CS) is a measure of the molecule loss from gas phase to the existing particle surface via condensation (Dal Maso et al., 2002; Kulmala et al., 2005). Modest source rates (Q) are enough for small particles to form and grow when the CS is low. However, when the CS is high, the vapour concentration needs to be higher in order for particles to form, grow, and survive to observable sizes (Kulmala et al., 2005). While CS can be a limiting factor for NPF, the occurrence of these NPF events at heavily polluted areas is an indication of high concentrations of condensable vapours. The vapour concentration (C_{vap}) needed to explain the growth was calculated using Eq. (8) in Nieminen et al. (2010) for sulphuric acid (H_2SO_4)

$$
C_{\text{vap}} = \frac{2\rho_v d_v}{\alpha_m m_v \Delta t} \sqrt{\frac{\pi m_v}{8kT}} \left[\frac{2x_1 + 1}{x_1(x_1 + 1)} - \frac{2x_0 + 1}{x_0(x_0 + 1)} \right.
$$
$$
\left. + 2\ln\left(\frac{x_1(x_0 + 1)}{x_0(x_1 + 1)}\right) \right].
\tag{2}
$$

Here, ρ_v is the condensed-phase density of the vapour, m_v its molecular mass, and d_v the diameter of the vapour molecule. α_m is the mass accommodation coefficient (assumed to be unity in the calculations), T the ambient temperature, and k the Boltzmann constant. In this equation, $x_1 = d_v/d_{p,\text{final}}$ and $x_0 = d_v/d_{p,\text{initial}}$. $d_{p,\text{initial}}$ refers to the initial particle diameter and $d_{p,\text{final}}$ refers to the final particle diameter after the time interval Δt. The equation provides the relationship between particle growth in time (Δt) and C_{vap} from $d_{p,\text{initial}}$ to $d_{p,\text{final}}$ for a given substance with a negligible saturation vapour pressure (H_2SO_4). To sustain the observed growth, the steady-state production rate (Q) of the condensing vapour was calculated as $Q = \text{CS} \cdot C_{\text{vap}}$.

The NPF event days and the formation rates of particles were determined according to the method described by Dal Maso et al. (2005). The formation rate (J) was calculated using particle concentrations in the size range 6–20 nm for the DMPS data and 2–3 nm for the NAIS data, denoted J_6 and $J_{2,\text{TOT}}$, respectively. The formation rate of 6 nm particles (J_6) was determined by

$$
J_6 = \frac{dN_6}{dt} + \text{CoagS} \cdot N_6 + \frac{\text{GR}}{\Delta d_p} \cdot N_6
\tag{3}
$$

according to Kulmala et al. (2012). Here, N_6 is the number concentration of 6–20 nm particles, CoagS is the coagulation sink of the pre-existing particles, Δd_p is the width of the 6–20 nm size range, and GR the growth rate of the particles in the same size range. CoagS is calculated from the particle

number size distributions with the method presented by Kulmala et al. (2001). For the growth-rate calculations we first determined the times of the concentration maxima in each of the size bins. Linear least-square fits were made to these points. The slope of these fits is the GR. A more thorough description of the method is given by Hirsikko et al. (2005) and Yli-Juuti et al. (2011).

The NAIS also measures naturally charged particles down to 0.8 nm in diameter, thus enabling us to observe the first steps of NPF events. The calculations of 2 nm ion formation rates (J_2) from 2–3 nm ion concentrations (of both polarities) were done according to Kulmala et al. (2012) as

$$J_2^\pm = \frac{dN_2^\pm}{dt} + \mathrm{CoagS} \cdot N_2^\pm + \frac{\mathrm{GR}}{\Delta d_\mathrm{p}} \cdot N_2^\pm + \alpha \cdot N_2^\pm \cdot N_2^\mp - \beta \cdot N_2 \cdot N_2^\pm \quad (4)$$

where the superscripts $\pm$ denote the particle charge. There are now two additional terms in comparison to Eq. (3). Additional losses for the ions occur via ion-ion collisions, was estimated assuming a recombination coefficient (α) value of 1.6×10^{-6} cm^3 s^{-1} (Tammet and Kulmala, 2005). Ion-neutral attachment was taken into account with the ion-neutral attachment coefficient (β) of 10^{-8} cm^3 s^{-1} (Tammet and Kulmala, 2005).

Sulphuric acid is closely linked to atmospheric NPF (e.g. Sipilä et al., 2011). As no measurements of sulphuric acid were done at the campaign site, we estimated the concentrations using the method presented by Petäjä et al. (2009). In steady-state conditions the proxy for sulphuric acid concentration is

$$H_2SO_4 = k \cdot [SO_2] \cdot \mathrm{GlobRad}/\mathrm{CS}. \quad (5)$$

Here, $[SO_2]$ is the sulphur dioxide concentration, GlobRad is solar radiation intensity, and CS the condensation sink by the pre-existing aerosol. For the scaling factor k, we used a value of $1.4 \times 10^{-7} \cdot \mathrm{GlobRad}^{-0.7}$ m^2 W^{-1} s^{-1}. This is based on measurements in a boreal forest environment in Finland (Petäjä et al., 2009), and, therefore, the absolute values should be considered as indicatory concentrations.

3 Results and discussion

The results presented were measured between 10 October 2010 and 10 January 2011 and are representative of the spring and early summer in São Paulo region. In spring, bursts of intense rainfall become gradually more frequent. This holds true for the measurement period and the transition from spring to summer in general. During summer months, rainfall culminates (Oliveira et al., 2003). During the period, there were 79 days with clear skies, 12 days with overcast clouds, and 23 rainy days. The remaining 14 days were days with a partial cloud-cover during the day.

All the times mentioned below are in Coordinated Universal Time (UTC) − 3 h, which is the local São Paulo wintertime and will be referred to as local time (LT).

3.1 Overview of the observed aerosol concentrations

Table 1 summarises the central aerosol parameters. From Table 1, it is evident that among the cities compared, the one that resembles São Paulo the most is Mexico City. Mexico City is also populated by roughly the same amount of people (20 million) and has almost the same population density (2800 km^{-2}) as São Paulo (2200 km^{-2}). The observed particle growth rates and particle number concentrations are similar. However, ω_0 at São Paulo was significantly lower than in Mexico City, so the aerosols may have different climatic impacts. In the work by Baumgardner et al. (2002), they stress the importance of the contribution by diesel vehicles, which are known to be strong BC sources. Moreover, the combustion of short-chained hydrocarbons (such as ethanol) is expected to result in less BC than the combustion of gasoline or diesel (Baumgardner et al., 2002). In general, Beijing has twice the concentrations we observed at São Paulo. Based on the comparison, also New Delhi has far worse air quality issues and airborne particulate matter than São Paulo.

The three-month average total particle number concentration was 2.35×10^4 cm^{-3} (standard deviation 1.04×10^4 cm^{-3}). This is roughly half of what has been measured in springtime in Beijing in 2004 (5.4×10^4 cm^{-3}, Wehner et al., 2004). In comparison, Hyvärinen et al. (2010) reported a mean concentration of 2.26×10^4 cm^{-3} for a rural site 25 km from the centre of New Delhi. The maximum 24-h average concentration during autumn in New Delhi (Mönkkönen et al., 2005) was twice as high (6.28×10^4 cm^{-3}, standard deviation 1.78×10^4 cm^{-3}) in comparison to 3.56×10^4 cm^{-3} (standard deviation 0.55×10^4 cm^{-3}), which we measured in São Paulo. During the course of weekdays, the range of the hourly median values of σ_{SP} and σ_{AP} was 21–57 Mm^{-1} and 13–35 Mm^{-1}, respectively. Using Eq. (1), the σ_{AP} range is equivalent to 2.0–5.4 µg m^{-3} of BC. This is in the same range ($\sigma_{SP} = 53$ Mm^{-1} and $\sigma_{AP} = 11$ Mm^{-1} mean values at 525 nm) as a remote site in northern India, mostly dominated by long range transport, i.e. the atmospheric brown cloud in Asia (Hyvärinen et al., 2009). The median σ_{AP} (and BC) were overall lower during weekends, between 9.2 and 30.3 Mm^{-1} (equivalent to 1.4–4.6 µg m^{-3} of BC).

3.2 Diurnal cycle of aerosol number concentrations

There was a clear diurnal pattern in the weekday total particle number concentration (Fig. 2a). The median concentration of the hour of the day varied between 1.6×10^4 and 2.1×10^4 cm^{-3} from midnight until 06:00 LT. When late night turned to early morning, there was a sharp increase in the total particle number concentration, which is likely due to vehicular emissions during the morning rush-hour. The highest total particle number concentrations were observed around noon. In the afternoon (13:00 LT onwards), the median concentrations slowly started to decline. During office

Table 1. Summary of observed, measured, and calculated aerosol parameters. The single values shown represent the averages and the two values the range of observations. The cities presented are São Paulo – Brazil, Beijing – China, New Delhi – India, Wukteshwar – India, and Mexico City – Mexico. The surroundings of the sites were classified into Urban (U), Sub-urban (S), and Remote (R) locations. N: number concentration, GR: growth rate, CS: condensation sink, σ_{AP}: absorption coefficient, σ_{SP}: scattering coefficient, ω_0 = single-scattering albedo. The optical properties are at $\lambda = 637$ nm unless stated otherwise below.

City/Average	N (10^4 cm^{-3})	GR (nm h^{-1})	CS (10^{-3} s^{-1})	σ_{AP} (Mm^{-1})	σ_{SP} (Mm^{-1})	ω_0 –
São Paulo (U)	2.35	9–25	6–17	12–33	21–64	0.59–0.76
Beijing[1,2,3] (U)	5.4	0.1–11	6–43	52	361	0.86
New Delhi[4,5] (S)	2.26	11–18	50–70	81	758	0.92
Mukteshwar[6,7] (R)	0.15–0.48	1–3	–	11	53	0.81
Mexico City[8,9] (U)	>2.1	6–18	–	7–33	50–175	0.75–0.92

[1] Wehner et al. (2004).
[2] Garland et al. (2009) σ_{AP} and ω_0 values are reported at 532 nm and σ_{SP} at 550 nm wavelengths.
[3] Wu et al. (2007).
[4] Mönkkönen et al. (2005).
[5] Hyvärinen et al. (2010) σ_{AP} and σ_{SP} reported at 520 and 670 nm wavelengths, respectively. ω_0 (at 670 nm) was estimated using a λ^{-1} wavelength dependency for σ_{AP}.
[6] Hyvärinen et al. (2009) σ_{AP} and ω_0 values are reported at 520 nm and σ_{SP} at 525 nm wavelengths.
[7] Neitola et al. (2011).
[8] Kalafut-Pettibone et al. (2011).
[9] Baumgardner et al. (2007) σ_{AP}, ω_0, σ_{SP} presumably at 565 nm wavelength.

hours (07:00–15:00 LT), the median concentrations reached up to 3.2×10^4 cm^{-3}. The drop in total particle number concentrations in the afternoon can also be partially explained by the heat island effect (discussed in more detail further on) and the geographical location of the measurement site at the western edge of the MASP. In the evening, the median values were typically 2.2×10^4 cm^{-3}. In the background of Fig. 2a, the 25th and 75th percentiles of the weekend data are shown in green (compare with the blue edges of the boxes for weekdays). The black whiskers in Fig. 2a mark the weekday 5th and 95th percentiles. Evidently, the weekend rush-hour occurred later than during the weekdays and was less intense. Thus, to isolate the traffic effects, we chose to focus the diurnal analysis on weekdays.

Wet deposition due to precipitation partly explains the lower extremes. The median particle number concentration during precipitation with an intensity of 3 mm h^{-1} or more was 1.4×10^4 cm^{-3}. The upper extremes of the particle number concentration originate from NPF events or by incidental nearby anthropogenic emissions (Allen et al., 2009; Hyvärinen et al., 2009, 2010).

Figure 2b presents the diurnal cycle of the median modal number concentration of the nucleation (6–25 nm), the Aitken (25–90 nm), and the accumulation mode (90–800 nm). The three modes were fitted to the size distributions using the method described by Hussein et al. (2005). The figure is restricted to weekdays only and split into cloudy and sunny days by comparing modelled and measured solar irradiance. Days with precipitation (23 of 93 days) were omitted in this plot because precipitation scavenges particles.

In Fig. 2b, cloud-cover and clear-sky number concentrations of nucleation-mode particles show a similar be-

haviour. However, the number concentrations were lower during cloudy days. During the early morning, there was a sharp increase from nighttime to rush-hour concentrations. Throughout the day, the clear-sky nucleation-mode concentrations were higher than during cloudy days. The concentration difference, especially around noon (10:00–14:00 LT), can be attributed to NPF events. In addition to NPF events, vehicular emissions are a source of nucleation-mode particles, profuse in urban areas. Otherwise, the diurnal cycles of the cloud-cover and clear-sky nucleation-mode concentrations were similar, except for the difference in concentrations.

The production of low vapour pressure species that are able to form and grow particles depends on photochemistry. The degradation of VOCs, a process that favours the accumulation of O_3 in the presence of NO$_x$, which in turn is a vital source of OH, depends on photochemistry (Jenkin and Clemitshaw, 2000; Kroll and Seinfeld, 2008). A pathway which favours the accumulation of O_3 is the photochemical dissociation of aldehydes (Seinfeld, 1989) or their reactions with OH radicals (Atkinson, 2000), which subsequently reacts with NO (Seinfeld, 1989; Tanner et al., 1988). Consequently, O_3 accumulates and allows for low vapour pressure species to be formed, as discussed in the introduction section. H_2SO_4 is also a product of photochemistry and closely linked to NPF and, therefore, nucleation-mode particles. Therefore, higher concentrations of nucleation-mode particles are expected during clear-sky conditions and in agreement with our observations. Direct measurement of the aerosol chemical composition would have been necessary to disclose the chemical composition of the aerosol, but was not available with the campaign instruments.
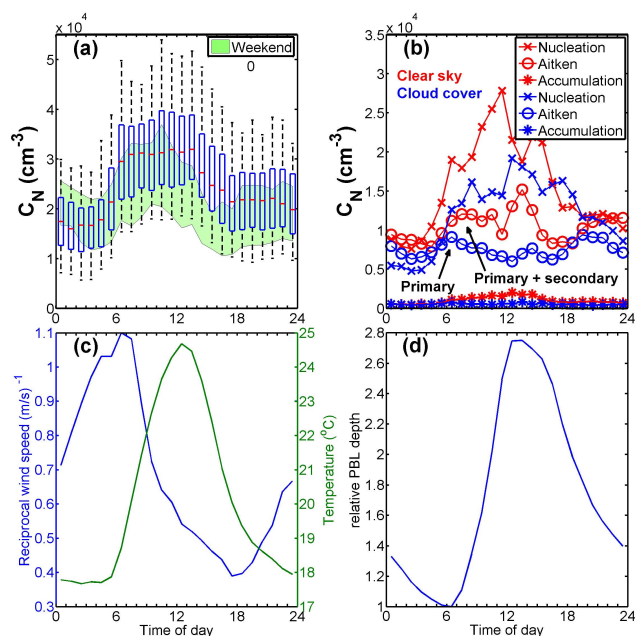
Fig. 2. Total particle number concentrations and the meteorological conditions affecting these. **(a)** Three month diurnal cycle of weekday total particle number concentrations (median values are in red). The upper and lower edges of the blue boxes are the 75th and 25th percentiles. The black whiskers indicate the 95th and 5th percentiles. In comparison, weekend total particle number concentration 75th and 25th percentile interval is shown in the background, in green. **(b)** Modal median number concentrations were obtained by fitting up to three modes to the number size distributions. Only weekday and precipitation free data are shown in this plot, distinguishing between cloudy and clear-sky days. **(c)** Diurnal reciprocal wind speed as a measure of atmospheric stagnation and diurnal temperature. **(d)** Modelled relative boundary layer depth from NOAA – CIRES 20th century reanalysis data at the nearest grid point to São Paulo (23.809° S, 46.875° W).

There is a notable difference in the diurnal cycles of the Aitken-mode particle number concentrations during clear-sky and cloud-covered conditions (Fig. 2b). During clear-sky morning rush hours, there was a gradual increase in the Aitken-mode particles from nighttime concentrations (median 0.8×10^4 cm^{-3} between 00:00 and 06:00 LT) until 10:00 LT (median 1.2×10^4 cm^{-3}). Furthermore, during cloud-covered conditions, the Aitken-mode peak concentration was more distinct (0.9×10^4 cm^{-3} between 06:00 and 07:00 LT) and declined until past noon (0.6×10^4 cm^{-3} between 12:00 and 13:00 LT). Arguably, we attribute the discrepancy to the change in photochemical activity, in the ultraviolet (UV) spectrum, suppressed by overcast conditions (Schafer et al., 1996). UV radiation is significantly reduced by overcast conditions, although less attenuated than the total solar irradiance (Estupinan et al., 1996). UV radiation is vital for generating degradation initiating oxidants yielding secondary aerosol mass (Crutzen and Zimmermann, 1991;

Seinfeld, 1989). The inorganic nitrates and sulphates common in urban aerosols depend on the production of H_2SO_4 and nitric acid (HNO_3) through photochemistry. Thus, we attribute the discrepancy to the secondary aerosol (inorganic and SOA) forming potential between the different conditions as indicated in Fig. 2b. The hypothesis is supported by the fact that the ground level O_3 concentrations, an indicator of photochemical activity in an urban environment (Jenkin and Clemitshaw, 2000), were on average 48 % lower during overcast conditions than during clear-sky conditions.

Past noon, both clear-sky and cloudy condition Aitken-mode particles had a second peak (between 13:00 and 14:00 LT for clear-sky conditions, and between 14:00 and 15:00 LT for cloud-covered conditions). Relative to the nucleation-mode particles the trend was opposite, suggesting that nucleation-mode particles had grown into the Aitken-mode. It further indicates an abundance of low or semi-volatile species. Again, the attenuation of UV radiation by clouds is the likely explanation for the difference between clear-sky and cloud-covered conditions.

The accumulation-mode number concentration peak occurred when the sun was directly overhead, at midday. During cloudy days (precipitation periods omitted), there was less of a difference between the nighttime low (440 cm^{-3} between 02:00 and 03:00 LT) and the midday peak concentrations (830 cm^{-3} between 13:00 and 14:00 LT). Clear-sky accumulation-mode particles peaked in the afternoon (2000 cm^{-3} between 12:00 and 13:00 LT) and accounts for only a small fraction of the total particle number concentration.

In the evening, especially after sunny days (18:00 LT and onwards), Aitken-mode particle concentrations had a number concentration increase, while nucleation-mode particle concentrations dropped (Fig. 2b). There was a shift from nucleation-mode particles to Aitken-mode particles as the largest contributor to total particle number concentrations. The physical processes that lead to the shift are favoured in the evening, as the PBL becomes shallow and air gradually stagnates (Fig. 2c, d). The reaction between NO_2 and O_3 form the NO_3 radical (Crutzen and Zimmermann, 1991), which will not photodissociate during nighttime, and is a potent scavenger of VOCs. Nighttime nitrogen chemistry can, therefore, produce low-volatile organic species by reactions with NO_3 radical (Crutzen and Zimmermann, 1991; Kroll and Seinfeld, 2008). Thus, pre-existing nucleation-mode particles can grow into the Aitken-mode regime as suggested from their inverse behaviour. In addition, sulphates and inorganic nitrates are likely to coat the particles too. The same behaviour has been reported for New Delhi. There, the geometric mean diameter (GMD) was low in the afternoon and increased into the night (Mönkkönen et al., 2005).

The accumulation of air pollution depends on the ground-level wind speed, i.e. the time interval in which the air mass resides at the pollution source (the MASP). During the measurement period, the average wind speed was 1.6 m s^{-1} with

a mean hourly variation from 0.9 to $2.6\,\mathrm{m\,s^{-1}}$, measured at the Osasco station (Fig. 1). The reciprocal wind speed (i.e. inverse wind speed) is a measure of air mass stagnation and thus a measure of the potential of air pollution accumulation. Figure 2c shows that the stagnation was the highest in the early morning (around 06:00 LT) and when the air mass starts to warm the air masses start moving.

The diurnal variation of ground level pollution is also governed by PBL depth and the stability of the PBL. During the measurement period, the PBL was convectively driven, as the predominance of moderate wind speeds (less than $4\,\mathrm{m\,s^{-1}}$) were unlikely to cause mechanically driven PBL mixing. To aid the interpretation of the aerosol observations we used the NOAA – CIRES 20th century reanalysis version 2 data (Compo et al., 2011) on PBL depth at the closest grid point (23.809° S, 46.875° W) in the reanalysis data set approximately 30 km away to the south west, at an elevation 900 m. The reanalysis data used was available until the end of 2010 and; therefore, the plot is based on modelled data from 10 October 2010 until 31 December 2010.

The stagnant air mass during early mornings and the shallow PBL exacerbate morning rush-hour pollution (Fig. 2c–d). These conditions help to build up aerosol pollution associated with primary emissions. Traffic is the main source of primary aerosol particles, being most intense during early office hours, as well as in the afternoon rush hour. At noon, the relative PBL height was modelled to be 2.8 times higher than between 06:00 and 07:00 LT. This is in agreement with an earlier study by Bischoff-Gauß et al. (1998) in the area. In the late afternoon, the air mass was on the move and the PBL depth was high (Fig. 2c–d). Then, convectional mixing of ground level pollution with the air mass above, throughout the PBL, will not favour the accumulation of ground level pollutants. Just after sunrise, when the air temperature starts to rise, the PBL height increases to a maximum at noon (Fig. 2d). Thus, PBL dynamics reflects observed aerosol number concentration diurnal patterns.

However, there were other factors playing in too. The measurement site was located at the western edge of the MASP. In the study by Oliveira et al. (2003), they conclude sea breeze, mountain valley circulation and urban heat island effects are the key features of the diurnal variations in air mass movement, in the MASP. The surface air within the city is warmer than the surrounding rural areas and, therefore, a heat island in comparison to its surrounding (Oke, 1982). This leads to warm air ascending at the centre of the heat island generating low level horizontal surface winds towards the centre from peripheral, rural areas (Kusaka and Kimura, 2004). Since the site was located at the western edge of the MASP, a heat island effect would show up as westerly winds especially during clear-sky conditions.

Figure 3a shows the mean diurnal wind direction measured at the Osasco monitoring station. In the afternoon (14:00–18:00 LT), during sunny days, there was an over 100° wind shift towards southwest, suggesting a heat island ef-
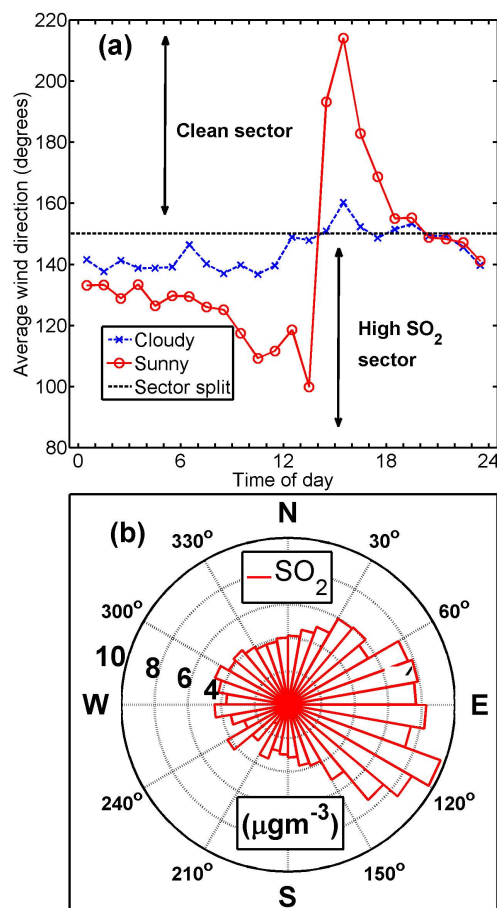
Fig. 3. The diurnal cycle of wind direction and wind direction dependence of SO₂. **(a)** Diurnal cycle of average wind direction and **(b)** the average sulphur dioxide (SO_2) mass concentrations measured at the Osasco monitoring station in each wind direction sector. The average wind direction was split into a clean sector and a sector associated with elevated concentrations of SO_2 indicated by the dashed line.

fect. SO_2 is linked to fossil fuel combustion and thus anthropogenic emissions. Figure 3b shows the SO_2 concentrations as a function of wind direction. Easterly winds originate from the geographical centre of the MASP and, therefore, exposed to anthropogenic emissions within the city, which explains the high SO_2 concentrations between 60° and 140° (Fig. 3b). The wind shift towards the low SO_2 sector is arguably the sector associated with less anthropogenic emissions. Bischoff-Grauß et al. (1998) showed that sea breeze (from the southeast) can reach the eastern suburbs of São Paulo and transport SO_2 from the industry area of Cubatão located at the slope Serra do Mar southeast of the measurement site. The magnitude of the contribution by the area remains unknown. Apparently, cloudy days were associated with winds from the southeast (Fig. 3a), possibly due to synoptic scale weather systems.

3.3　Diurnal cycles of aerosol optical properties

Aerosol optical properties are known to be of climatological significance (e.g. Haywood and Boucher, 2000; Haywood and Shine, 1995). The diurnal cycles of the aerosol optical properties and O_3 are shown in Fig. 4. Most notably, during stagnant atmospheric conditions there was a morning rush-hour peak in σ_{AP} (and BC). Between 06:00 and 08:00 LT, median σ_{AP} peaked at 35 Mm^{-1} (equivalent to 5.3 µg m^{-3} of BC according to Eq. 1) during weekdays. Both coefficients had minima in the afternoon (Fig. 4a–b). In the afternoon, the weekday median σ_{AP} dropped to 13.8 Mm^{-1} (12:00–13:00 LT), i.e. the morning rush-hour concentrations were 2.5 times higher. The growth of the PBL height (Fig. 2d) mixes ground level pollutants throughout the PBL and thus explains the observed decrease in σ_{AP}. At noon, the relative PBL height was 2.8 times higher than between 06:00 and 07:00 LT and consistent with the observed drop in σ_{AP}.

The weekday σ_{SP} also had a morning rush-hour peak, however, one hour later (08:00–09:00 LT) than σ_{AP}. While aerosol light absorption is dominated by BC particles, light-scattering species are mostly of secondary origin such as sulphates, nitrates, and SOA. These groups are governed by the atmospheric reactivity of their precursors, and thus the concentration of the initiating oxidants which affects the secondary aerosol yield. Consequently, increased atmospheric reactivity will favour the accumulation of secondary aerosol mass and eventually impact light scattering coefficients. The formation and accumulation of nitrous acid (HONO) during the night is a known source of OH radicals when it photodissociates at sunrise. Subsequently, this leads to OH and HO_2 radicals during early mornings (Aumont et al., 2003; Jacob, 2000), prior to the accumulation of O_3 which is a main contributor of OH radicals during the day. These oxidants and the following sequence of reactions are likely contributors to the increase in σ_{SP} through secondary aerosol formation, however, one hour later than for the primary aerosol driven σ_{AP}, during the early morning rush hours. Weekday σ_{SP} peaked at 08:00–09:00 LT ($\sigma_{SP} = 57.0$ Mm^{-1}). As was the case for the Aitken-mode particles (Fig. 2b), σ_{SP} also had a somewhat smaller midday peak (37.2 Mm^{-1}, 13:00–14:00 LT).

Similar morning rush-hour peaks have been observed in, for example, Mexico City (Baumgardner et al., 2007; Paredes-Miranda, 2009) and Beijing (Garland et al., 2009). All report the highest light absorption and light scattering coefficients during morning rush hours and the lowest coefficients in the afternoon. In the study by Baumgardner et al. (2007) the absorption coefficient reached just above 30 Mm^{-1} measured with a Particle Soot Absorption Photometer (presumably at a wavelength of 565 nm). This is somewhat lower than the median 35 Mm^{-1} we obtained (at a wavelength of 637 nm) considering an assumed λ^{-1} wavelength dependency. By using a more sophisticated measurement technique, they showed the average coating thickness to
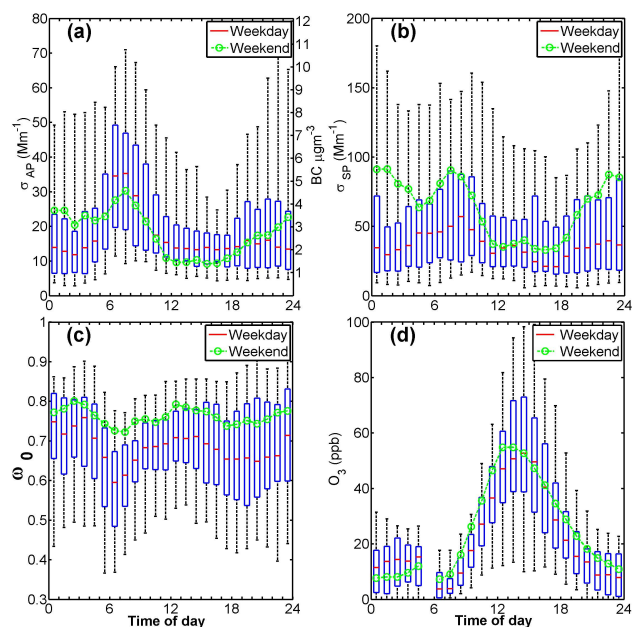
Fig. 4. The diurnal cycle of aerosol optical properties and O_3. Diurnal weekday cycle of **(a)** light absorption coefficients and BC mass concentrations (on the right y-axis), **(b)** light scattering coefficients, **(c)** single-scattering albedo at 637 nm and **(d)** ozone (O_3) concentrations. The edges of the blue boxes represent the 75th and 25th percentiles and the black whiskers the 95th and 5th percentiles. Weekday diurnal median values are in red and weekends in green.

be the smallest during early mornings and thickest just past noon.

When BC particles get coated with sulphates, nitrates and organics their single-scattering albedo (ω_0) increases, since these are light scattering species. In the morning, ω_0 was at its lowest (Fig. 4c), especially during weekday mornings ($\omega_0 = 0.59$ between 06:00 and 07:00 LT) and peaked in the afternoon ($\omega_0 = 0.71$ between 14 and 15:00 LT for weekdays). The diurnal ω_0 maximum 0.76 occurred at night, between 03:00 and 04:00 LT. The minimum was consistent with the absorption peak discussed earlier, indicating a significant fraction of BC mass. During morning rush hour, the nocturnal boundary layer had not yet broken up (Fig. 2d), while traffic was heavy. When it broke up, the primary BC was diluted due to convectional mixing, and σ_{AP} decreased at ground level. At the same time, photochemistry becomes relevant and will cause gas-phase pollutants to partition between the gas phase and the condensed phase, thus coating the pre-existing particles, increasing the overall ω_0. Secondary aerosol formed through the photodissociation of HONO (which releases OH) is a likely contributor to the early morning increase in ω_0 (Fig. 4c, between 06:00 and 08:00 LT for weekdays), whereas O_3 (which is also a source of OH) is expected to play a crucial role during the day in affecting the ω_0 of the aerosol.

In the evening, there was a gradual decrease in ω_0, coinciding with the evening rush hour. Nighttime atmospheric conditions are most stable and stagnant during the night. After sunset, NO_3 is formed (Crutzen and Zimmermann, 1991) which is a known nighttime scavenger of organics and forms organic nitrates (Hallquist et al., 2009). Nighttime NO_3 will contribute to additional secondary aerosol mass and thus increase the ω_0 of the aerosol. In the stable nocturnal PBL, the process can be observed for a longer period than during sunlight hours, which is why ω_0 has its highest value at night (between 03:00 and 04:00 LT).

There is a difference in ω_0 during weekdays and weekends. On the average, weekend ω_0 was 0.072 higher than on weekdays (0.706 for weekdays and 0.778 for weekends). A partial explanation would be less heavy-duty diesel vehicles on the road during weekends. However, this does not explain the higher σ_{SP} during weekends (Fig. 4b).

Chemical transport models have shown a coupling between O_3 and particulate matter in an urban environment (Meng et al., 1997). Thus, O_3 is also linked to the optical properties of the aerosol through secondary aerosol formation. Although studies have shown that a high ethanol blend can reduce NO_x emissions by 45 % (Graham et al., 2008) the model run by Meng et al. (1997) predicts only a minor change in O_3 and $PM_{2.5}$ levels, given only NO_x is reduced. The study by Jang and Kamens (2001) points out the role of heterogeneous chemistry between the gas phase aldehyde functional groups and particulate matter in the presence of an acid catalyst, e.g. H_2SO_4. Furthermore, they argue that considering the vapour pressures of atmospheric aldehydes (with less than eight carbons) they are unlikely to be accommodated in the condensed-phase unless they first undergo heterogeneous reactions. Jacob (2000) points out the possibility of organic carbon aerosols as sinks for O_3 since they have a high reactivity towards O_3. The rates at which these heterogeneous and multiple phase reactions become relevant for ω_0 through a gain in secondary aerosol mass at the site remains unknown. Although both O_3 concentrations and ω_0 peak at the same time during the day (Fig. 4c, d), the ω_0 at the site was considerably lower than for the other cities listed in Table 1. A gain in secondary aerosol mass will increase the ω_0 of the aerosol. The low ω_0 of the aerosol, in comparison to the other sites, is likely a consequence of less secondary aerosol mass (organic and inorganic) present in the aerosol at the site. It suggests that the formation of secondary aerosol mass from ethanol combustion associated emissions can be slow, in comparison to sites with little or no ethanol usage, since increased aldehyde emissions have previously been linked to the formation of photochemical smog (Haagen-Smit, 1952; Tanner et al., 1988; Atkinson, 2000).

According to Ramanathan et al. (2001), ω_0 values below 0.85 result in a TOA positive climate forcing in general. Although strongly dependent on ω_0, the radiative properties of an aerosol burden layer also depends on surface reflectance, cloud cover and the upscatter fraction (β) of the aerosol, (Haywood and Boucher, 2000; Haywood and Shine, 1995; Ramanathan et al., 2001). According to Oke (1988), the surface reflectance for urban areas is on average 0.14 ranging between 0.09 and 0.27. Haywood and Shine (1995) report the critical single-scattering albedo ω_{crit} at a given β. In the case of $\omega_0 < \omega_{crit}$, the TOA radiative forcing is positive (i.e. warming of the atmosphere). Considering the low surface reflectance of urban areas, for the given range of ω_0, the TOA radiative forcing effect can be either positive or negative for the sources within the MASP. Since backscattering coefficient were not measured it is not possible to calculate ω_{crit} for the data set. Another climatic effect of low ω_0 is related to the fact that they may affect the vertical temperature structure in the lower troposphere with implications to atmospheric convection and cloud formation (Hansen et al., 1997; Herrmann and Hanel, 1997). Satheesh et al. (2010) show that a polluted continental aerosol layer will increase the temperature of the atmosphere and thus reduce it at the surface.

Further studies on how ω_0 evolves downwind of the city are needed to uncover the true climatic implications for the aerosol pollution enforced by the sources within the MASP. Acetaldehyde, which is formed during ethanol combustion, can form peroxyacetyle nitrate (PAN) in the presence of NO_2 (Tanner et al., 1988). The reaction is reversible which can lead to the formation O_3 downwind of the source with possible implications on the aerosol optical properties.

3.4 Observed evaporation of submicron aerosol

The growth of particles by condensable vapours depends on their concentration. Degradation initiating oxidants are able to start reactions which lower the saturation vapour pressure of gas-phase pollutants. As discussed earlier, the oxidation process will make them more likely to condense. If the condensational growth of the particles stops, the condensation and evaporation processes are at steady state. Should the atmospheric conditions change in a way that the concentration of the precursor vapour decreases (e.g. PBL growth), the condensed semi-volatile species start to evaporate, and thus making the particles shrink in size. Other mechanisms may also cause particle mass to evaporate. For instance, the reversible reaction of ammonia (NH_3) and HNO_3 produces ammonium nitrate (NH_4NO_3) that is a well-known constituent of aerosol particles. The amount of particulate NH_4NO_3 depends on the $HNO_3/NH_3/NH_4NO_3$ equilibrium. If HNO_3 levels drop the equilibrium can be shifted to favour the gas phase causing particulate NH_4NO_3 to evaporate.

On 12 October 2010, we observed ambient submicron particle modes decrease in size, between 14:00 and 17:00 LT (Fig. 5). We can see that the existing population of 36 nm particles shrank, likely by evaporation, to 16 nm (Fig. 5). The rate of shrinking was calculated to be $5.2 \, \mathrm{nm \, h^{-1}}$. The shrinking of the accumulation-mode particles can also be seen, however, not as clearly, starting before noon. The global irradiance data suggest that during morning hours,
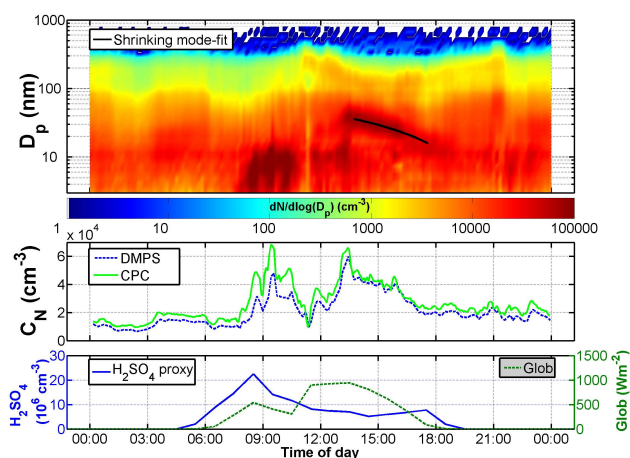
Fig. 5. Class II type event during morning hours and a shrinking mode in the early afternoon on 12 October 2010. The evaporation rate of the shrinking mode was calculated to be $5.2\,\mathrm{nm\,h^{-1}}$ (upper panel). The split between NAIS and DMPS data in the picture is at 15 nm. During the evaporation (from 14:00 to 17:00 LT) the total particle concentration (C_N) declines constantly (middle panel). In the middle panel, DMPS concentrations between 6 and 800 nm and CPC concentrations between 5 nm and 2.5 μm are shown. The lower panel shows the H_2SO_4 proxy concentration, and global irradiance (Glob).

until 11:00 LT, it was partly cloudy (Fig. 5) and after 12:00 LT there was little or no cloud cover. Either a stable nocturnal boundary layer broke up, or the boundary layer mixing height increased. This would dilute ground-level total particle concentrations and the trace-gas levels thus explaining the observed evaporation. Aerosol mass spectrometer measurements would be vital in order to give a conclusive explanation for the observed evaporation.

3.5 Weekly patterns

The total particle number concentration and BC mass concentrations as a function of the day of the week is shown in Fig. 6. In general, the weekend particle number concentrations were lower than during weekdays, because there is less traffic during weekends (Silva Júnior et al., 2009). Sunday had the lowest and Friday the highest median particle number concentrations, 1.78×10^4 and $2.53 \times 10^4\,\mathrm{cm^{-3}}$ respectively (Fig. 6a). A similar weekly cycle can also be seen for BC (Fig. 6b). BC concentrations were the lowest on Sundays ($1.1\,\mathrm{\mu g\,m^{-3}}$) and the highest on Fridays ($2.7\,\mathrm{\mu g\,m^{-3}}$). Seemingly, Saturdays were busy in terms of traffic and pollution associated with it. However, since Friday shows the highest concentrations (Fig. 6) there were likely carryovers from Friday to Saturday which, at least partly, explain the elevated concentrations on Saturday. This argumentation is supported by Fig. 2a which show elevated total particle number concentrations during late night on weekends (half of which are Saturdays). This same diurnal cycle is also evi-
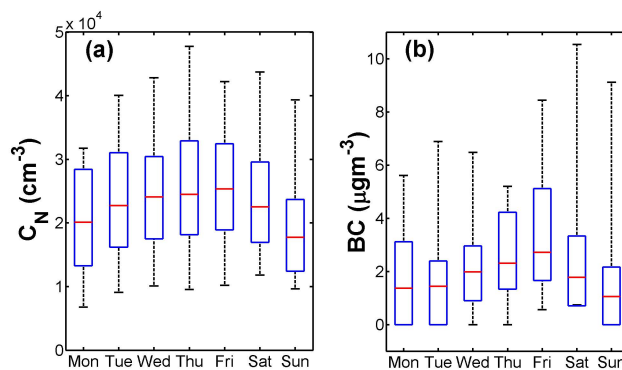

Fig. 6. The weekly cycle of total particle number concentrations and BC. Median values are in red, 75th and 25th percentiles in blue and 95th and 5th percentiles as black whiskers. **(a)** The weekly cycle of the total particle number concentration. Sundays had the lowest and Fridays the highest concentrations, 1.78×10^4 and $2.53 \times 10^4\,\mathrm{cm^{-3}}$, respectively, at STP conditions. **(b)** Median BC mass concentrations show a similar pattern with the lowest median value of $1.06\,\mathrm{\mu g\,m^{-3}}$ on Sundays, and the highest on Fridays $2.71\,\mathrm{\mu g\,m^{-3}}$.

dent from Fig. 4a–b showing BC mass concentrations and light scattering coefficients. Furthermore, there seems to be distinctively different traffic patterns during weekends and during weekdays (e.g. weekend evening BC concentrations were higher than during weekdays). The higher concentrations are not necessarily related to more traffic, but rather to traffic during a stable nocturnal boundary layer and in stagnant air (Fig. 2c, d).

Vehicular emissions are a known source of nucleation-mode particles in urban environments (e.g. Kittelson et al., 2004; Sturm et al., 2003; Zhu et al., 2002). Subsequently, physical processes will shape the size distribution of the vehicular emissions which has been the focus of a number of studies (e.g. Kerminen et al., 2004; Kittelson, 2004; Wehner et al., 2002; Zhu et al., 2002). These studies have shown, however, to a varying degree, the persistence of the nucleation mode. Therefore, three log-normal modes were fitted to the size distributions (Fig. 7) using the method described by Hussein et al. (2005). Figure 7 shows the median particle number size distribution for weekdays and weekends. The distribution is the median concentration of each size-segment separated into weekdays and weekends.

During weekdays, nucleation-mode particles contributed the most to the total particle number concentration. Their median concentration was $11\,500\,\mathrm{cm^{-3}}$, whereas the medians of the Aitken-mode and accumulation-mode particle concentrations were $9300\,\mathrm{cm^{-3}}$ and a $610\,\mathrm{cm^{-3}}$, respectively. During weekends, the median concentrations of the nucleation and Aitken mode particles were roughly the same, 9400 and $9000\,\mathrm{cm^{-3}}$, respectively. The median concentration of the accumulation-mode particles on weekends was $640\,\mathrm{cm^{-3}}$. The modal peak of the weekday nucleation mode was at
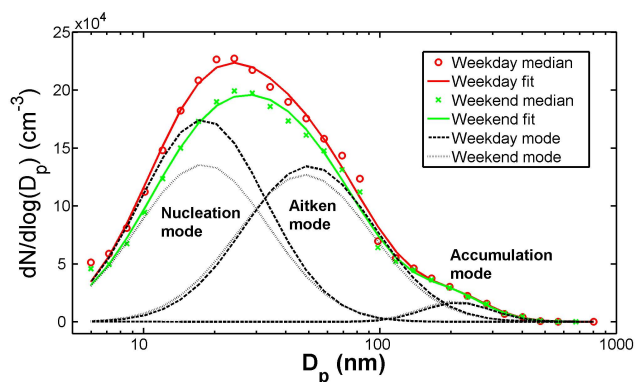
Fig. 7. Three month median number size distribution with three modes fitted to the data. Weekday (weekend) modal peaks of the nucleation, Aitken, and accumulation mode particles are at 18 (18), 50 (48) and 213 (206) nm, respectively. Weekday (weekend) median modal particle concentrations are 11 500 (9400), 9300 (9000) and 610 (640) cm^{-3}. The widths (σ) of the mode fits are 1.83 (1.89), 1.89 (1.92) and 1.40 (1.40).

18 nm. Weekday Aitken mode particles peak at 50 nm and accumulation mode at 213 nm. During weekends, nucleation, Aitken and accumulation mode particles peak at 18, 48 and 206 nm. Weekday (weekend) widths of the log-normal distributions (σ) were calculated to be 1.83 (1.89) for nucleation mode, 1.92 (1.92) for Aitken mode and 1.40 (1.40) for the accumulation mode particles. The peak of the median particle number size distribution was at 24 nm during weekdays and at 29 nm during weekends.

3.6 New particle formation events

In addition to vehicular emissions, NPF events are a source of nucleation-mode particles. 10 NPF events were observed during 93 days (Table 2). They were classified into three classes. NPF events where growth was observed from the start, and the freshly formed particle grew continuously for several hours were classified as Class Ia events. Events which showed a growth of nucleation-mode particles, however, not from the beginning, were classified as Class Ib. Class II events were events for which no growth of the formed nucleation-mode particles could be calculated. In brief, this is the procedure for classifying described by Dal Maso et al. (2005), for regional nucleation events. Four class Ia events could be further analysed. The Class Ib events were likely local NPF events passing by the measurement station which would explain the absence of the initiation of the event. Two Class II type events were observed (Table 2). The rest of the days were classified as non-event days.

The most intense (i.e. the highest $J_{2,\text{TOT}}$ formation rate) NPF event observed had a GR of 9.3 nm h^{-1}. The particle number size distributions measured during the event are presented in Figs. 8 and 9. The event begins at 09:00 LT. The fast growth of the particles resulted in that the event showed
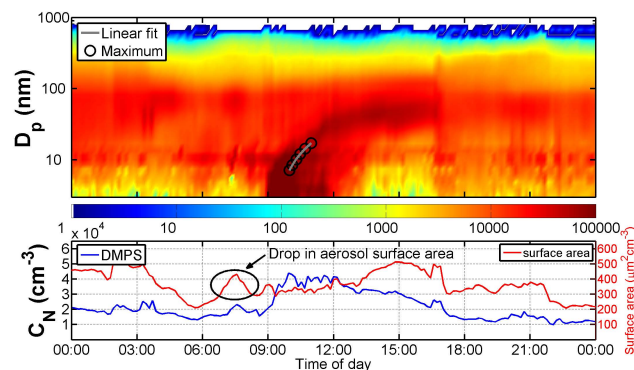
Fig. 8. The nucleation event measured on 2 November 2010. A growth rate (GR$_{6-20}$) of 9.3 nm h^{-1} was calculated using DMPS data from 6 to 20 nm. The black circles in the upper panel indicate peaks of the size distribution. The split between NAIS and DMPS data in the picture is at 15 nm.
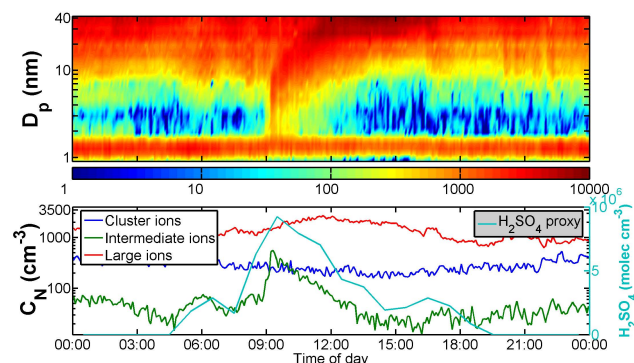
Fig. 9. The nucleation event measured on 2 November 2010 by the NAIS and the H$_2$SO$_4$ proxy concentration. The upper panel shows naturally positively charged particle number size distribution (0.8–42 nm) measured with the NAIS on 2 November 2010. The lower panel shows number concentrations of cluster (< 1.8 nm), intermediate (1.8–7 nm) and large (7–42 nm) ions. The sulphuric acid (H$_2$SO$_4$) proxy concentration is shown on the right axis.

up roughly the same time in both the DMPS and the NAIS. In Fig. 8, we can see a similar drop in total aerosol surface area before the event begins as was reported for Beijing, China (Wehner et al., 2004). The sulphuric acid proxy concentration (H$_2$SO$_4$) is shown in the lower panel of Fig. 9. The proxy concentration was calculated using Eq. (5). The H$_2$SO$_4$ proxy started to increase already at 08:00 LT, an hour earlier than the NPF event. Later, when the H$_2$SO$_4$ proxy concentration decreased just before noon, no new particles were formed, while the freshly nucleated particles continued to grow into larger sizes. There are a couple of possibilities for this behaviour. Either there was a H$_2$SO$_4$ concentration threshold of approximately 5×10^6 cm^{-3} or the trace gas monitoring station further away measured another air mass (time delay). Another uncertainty is the conversion technique itself since it is based on a parameterisation

Table 2. Summary of observed new particle formation events between 10 October 2010 and 10 January 2011. They were classified according to Dal Maso et al. (2005). The growth rates (GR) and particle fluxes (J) with two values were calculated from ion spectrometer data for both polarities ($+$ and $-$). $J_{2,\text{TOT}}$ was calculated from corona-charged (negative) particles. The condensation sink (CS), vapour concentration (C_{vap}) and production rates (Q) were calculated from DMPS data. The H_2SO_4 proxy was calculated from SO_2 data (Petäjä et al., 2009).

Date	Type	GR_{1-3} $(+/-)$	GR_{3-7} $(+/-)$	GR_{7-20} $(+/-)$	GR_{6-20}	J_2 $(+/-)$	$J_{2,\text{TOT}}$	J_6	CS	C_{vap} H_2SO_4	H_2SO_4 proxy	Q
		(nm h^{-1})				(cm^{-3} s^{-1})			(10^{-3} s^{-1})	(10^8 cm^{-3})	(10^7 cm^{-3})	(10^6 cm^{-3} s^{-1})
10 Oct	Ia	7.0/8.0	14.1/8.3	48.5/33.8	25.1	0.13/0.08	10.3	11.2	5.7	4.3	1.4	2.5
12 Oct	II	–	–	–	–	–	–	–	–	–	–	–
31 Oct	Ib	–	–	–	–	–	–	–	–	–	–	–
2 Nov	Ia	6.1/4.7	5.3/–	7.0/7.2	9.3	0.25/0.04	55.7	11.4	16.7	1.6	0.9	2.7
3 Nov	Ib	–	–	–	–	–	–	–	–	–	–	–
7 Nov	Ia	6.3/4.1	10.3/5.8	12.5/10.8	16.1	0.25/0.12	23.1	18.5	15.7	2.8	1.1	4.4
15 Nov	Ia	5.0/3.9	16.9/7.1	14.1/5.7	10.7	0.14/0.08	10.3	4.5	9.9	1.8	1.1	1.8
12 Dec	Undef.	–	–	–	–	–	–	–	–	–	–	–
31 Dec	II	–	–	–	–	–	–	–	–	–	–	–
1 Jan	Ib	–	–	–	–	–	–	–	–	–	–	–
Mean		6.2/4.4	12.2/7.1	13.3/9.0	15.3	0.19/0.08	24.9	11.4	12.0	2.6	1.1	2.8

for a different site. Furthermore, when there were no more nucleating vapours, the solar irradiation still increased to a maximum between 11:00 and 12:00 LT. The decline in the sulphuric acid proxy between 09:00 and 10:00 LT was due to less SO_2, not solar irradiation. Increasing mixing height due to thermal convection, as the day grew older, mixed the ground-level SO_2 throughout the boundary layer. This reduced SO_2 concentrations, and consequently H_2SO_4 proxy concentrations, which are closely linked to NPF events.

Since the trace gas monitoring station (used to derive the H_2SO_4 proxy) was some 6 km away from the measurement site, it adds uncertainties to both the timeframe and absolute concentrations. However, as the timing of the H_2SO_4 proxy and the NPF event match, we can expect to have nucleating particles at both stations. At a boreal forest environment in Finland, Nieminen et al. (2009) reported an order of magnitude lower threshold concentration of 3×10^5 cm^{-3} based on measured H_2SO_4. The H_2SO_4 concentration needed to explain the growth, calculated using Eq. (2) was on the average, 2.6×10^8 cm^{-3} for São Paulo (Table 2). The average H_2SO_4 proxy concentration was over an order of magnitude less (1.1×10^7 cm^{-3}). However, still considering the uncertainties, there were most likely other vapours (e.g. organics) present in these NPF events contributing to particle growth (Jimenez et al., 2009; Orlando et al., 2010; Zhang, 2010). This is consistent with observations at other locations (e.g. Kulmala et al., 2001; Wehner et al., 2005).

A summary of the parameters derived from the NPF events as described in the methods section of this paper is given in Table 2. We chose to compare the results with results from New Delhi, India (Mönkkönen et al., 2005), Beijing, China (Wehner et al., 2004), and Mexico City Mexico (Dunn et al., 2004; Kalafut-Pettibone et al., 2011). In São Paulo, we observed GRs between 9 and 25 nm h^{-1}. In New Delhi, India similar GRs have been observed (11–18 nm h^{-1}, Mönkkönen et al., 2005). For Beijing, lower

growth rates have been reported (Wu et al., 2007). Also for Mexico City similar GRs have been reported ranging from 6 to 18 nm h^{-1} (Kalafut-Pettibone et al., 2011). This is an order of magnitude higher GRs than what has been reported for a remote site in the Indian Himalayas (Neitola et al., 2011). Mönkkönen et al. (2005) reported NPF with a CS in the range of $50–70 \times 10^{-3}$ s^{-1} which is by a factor of 3–11 more than what was measured in São Paulo (in the range of $6–17 \times 10^{-3}$ s^{-1}). Similarly, the vapour production rate in New Delhi (9×10^6–14×10^6 cm^{-3} s^{-1}) was up to one order of magnitude more than for São Paulo (1.5–3.5×10^6 cm^{-3} s^{-1}). In contrast to NPF in pristine conditions (e.g. Dal Maso et al., 2005), we observed NPF events with a much higher pre-existing aerosol population of 2×10^4 cm^{-3} on 2 November 2010 (Fig. 8).

4 Summary and conclusions

The MASP has a population of 20 million and a vehicular fleet of 8.4 million, which is one fifth of the Brazilian vehicular fleet (CETESB, 2007). Although megacities cover a small area of land they have wide spread implications on the hydrological cycle, health and even the regional climate (IPCC, 2007; Lohmann and Feichter, 2005; Nel, 2005). Demographic differences between cities result in a different pollution burden (Gurjar et al., 2008). A feature of the area is the use of bioethanol by the vehicular fleet. Ethanol as vehicle fuel results in increased acetaldehyde and formaldehyde emissions which favours the formation of O_3 (Atkins, 2000; Graham et al., 2008; Seinfeld, 1989). The formation of O_3 has a central role in the production of degradation initiating oxidants responsible for the photochemical smog which is characteristic for polluted areas (Atkinson, 2000; Jenkin and Clemitshaw, 2000; Kroll and Seinfeld, 2008).

Particle number size distributions, total particle number concentrations, BC mass concentrations, and aerosol optical

properties were tracked to uncover the diurnal cycle of the particulate submicron aerosol pollution in the MASP. In addition to the campaign aerosol instrumentation, data from existing measurement stations were used to aid the interpretation of the measurements, such as meteorological parameters and trace gas measurements. Furthermore, NOAA – CIRES 20th century reanalysis version 2 PBL height data were used to aid the interpretation of the measurements.

Ground level aerosol concentrations were found to be governed by meteorological conditions. Standing air favoured the accumulation of primary aerosol pollutants within the MASP. Using wind speed data and modelled PBL depth we found the air mass to be the most stagnant during early mornings, then the PBL depth is the shallowest. These conditions exacerbate air quality during the early morning rush hour. After dawn, the PBL depth increases when the air warms and the air mass begins to move. During clear-sky conditions, a $100°$ wind shift away from the geographical centre of MASP indicated there is a heat island effect which affects the measurement site. The wind shift leads to lower concentrations of SO_2 which are associated with anthropogenic emissions.

The aerosol properties tracked showed clear diurnal cycles related to emission sources, photochemistry and meteorology. Typically, the median total particle number concentration of the hour of the day varied between 1.6 and 2.2×10^4 cm^{-3}, during nighttime. During office hours, the median total particle concentrations reached up to 3.2×10^4 cm^{-3}. During weekdays, the nucleation-mode particles 6–25 nm make up most of the particles by numbers (1.15×10^4 cm^{-3}) and Aitken-mode particles (25–90 nm) account for most of the rest (0.93×10^4 cm^{-3}) with only a minor contribution by accumulation-mode particles (610 cm^{-3}). During clear-sky conditions, total particle concentrations were higher, since the formation of low vapour pressure compounds that are able to form and grow aerosol particles depends on photochemistry. During clear-sky conditions, nucleation-mode particles were more likely to grow into Aitken-mode sizes, suggested by their inverse particle concentration behaviour.

The aerosol optical properties suggest that early morning aerosol pollution was traffic related. σ_{AP} peaked between 06:00 and 08:00 LT (35 Mm^{-1} equal to 5.3 µg m^{-3} at 637 nm wavelength). The diurnal cycle of the PBL depth was consistent with the observed drop in the primary aerosol drive σ_{AP}, indicating the mixing of primary aerosol pollutants throughout the PBL. At the same time σ_{AP} peaked, ω_0 had a minimum (0.59). σ_{SP} peaked one hour later between 08:00 and 09:00 LT (57 Mm^{-1} at 637 nm wavelength) indicating a gain in secondary aerosol mass and thus increasing the ω_0 of the aerosol. O_3 is an indispensable source of OH radicals which are vital for the processes that lead to a secondary aerosol mass gain by the aerosol, thus changing the optical properties of the aerosol. At the same time O_3 concentrations peaked just after noon, ω_0 peaked at 0.71. The average ω_0 was 0.706 for weekdays and 0.778 for weekends. This suggests a di-

rect TOA net warming effect by the aerosol layer in general. However, considering the low surface reflectance of urban areas, and the range of ω_0, the direct radiative forcing is likely to change sign within the MASP. Further studies on how ω_0 evolves downwind of the city could reveal the direct climatic implications of the city on a broader scale. The higher weekend values are likely due to less commercial diesel vehicles on the road.

The comparison between different megacities (Table 1) shows that Mexico City is the city that most resembles the MASP. The population base is comparable to the 20 million inhabitants in the MASP. The population density of Mexico City is 2800 km^{-2} and 2200 km^{-2} for São Paulo. Consistently, the observed particle growth rates at both sites are also similar and so are the total particle number concentrations. Further studies are needed to be able to compare the different radiative forcing potentials of the cities. The Asian megacities Beijing and New Delhi have far worse air quality issues and airborne particulate matter than São Paulo. The comparison shows a significantly lower ω_0 for the MASP aerosol. In comparison to the other cities, the low ω_0 of the MASP aerosol is likely due to less secondary aerosol mass present at the site. A gain in secondary aerosols mass will increase the σ_{SP} of the aerosol. For example, when comparing MASP and Mexico City, the σ_{AP} values reported for both sites are in the same range, whereas σ_{SP} values reported for Mexico City are more than double (Table 1). If the conversion processes, which lead to the formation of secondary aerosol mass, are slower for ethanol combustion associated pollutants, than for those associated with gasoline combustion, it would consequently lead to a lower ω_0 for the MASP aerosol.

During the 93 days of measurements, NPF events were observed on 11 % of the days. During the events, the growth rates ranged between 9 and 25 nm h^{-1}. We calculated H_2SO_4 proxy concentrations using SO_2, global irradiance and particle number size distribution data. On the average, a sulphuric acid vapour concentration of at least 2.6×10^8 cm^{-3} would have explained the observed growth. However, the H_2SO_4 concentrations were typically not high enough solely to explain the growth. The H_2SO_4 proxy estimate was on the average 1.1×10^7 cm^{-3}, accounting for less than 5 % of the concentration needed, given all condensing vapour is H_2SO_4. Even after taking the uncertainties into account, the data suggest other vapours were likely to contribute to particle growth.

Based on these results we decided to continue the measurements in the city of São Paulo since more experimental evidence is needed to corroborate these observations.

Edited by: R. Krejci

References

Aalto, P. P., Hämeri, K., Becker, E., Weber, R., Salm, J., Mäkelä, J. M., Hoell, C., O'Dowd, C. D., Karlsson, H., Hansson, H. C., Väkevä, M., Koponen, I. K., Buzorius, G., and Kulmala, M.: Physical characterization of aerosol particles during nucleation events, Tellus B, 53, 344–358, 2001.

Agarwal, J. K. and Sem, G. J.: Generating Submicron Monodisperse Aerosols for Instrument Calibration, TSI Quarterly, 4, 2–8, 1978.

Allen, A. G., McGonigle, A. J. S., Cardoso, A. A., Machado, C. M. D., Davison, B., Paterlini, W. C., da Rocha, G. O., and de Andrade, J. B.: Influence of Sources and Meteorology on Surface Concentrations of Gases and Aerosols in a Coastal Industrial Complex, J. Braz. Chem. Soc., 20, 214–221, 2009.

Anderson, T. L. and Ogren, J. A.: Determining aerosol radiative properties using the TSI 3563 integrating nephelometer, Aerosol. Sci. Technol., 29, 57–69, 1998.

Andreae, M.: The dark side of aerosols, Nature, 409, 671–672, doi:10.1038/35055640, 2001.

Atkinson, R.: Atmospheric chemistry of VOCs and NO$_x$, Atmos. Environ., 34, 2063–2101, doi:10.1016/S1352-2310(99)00460-4, 2000.

Aumont, B., Chervier, F., and Laval, S.: Contribution of HONO sources to the NOx/HOx/O-3 chemistry in the polluted boundary layer, Atmos. Environ., 37, 487–498, doi:10.1016/S1352-2310(02)00920-2, 2003.

Baumgardner, D., Raga, G., Peralta, O., Rosas, I., Castro, T., Kuhlbusch, T., John, A., and Petzold, A.: Diagnosing black carbon trends in large urban areas using carbon monoxide measurements, J. Geophys. Res.-Atmos., 107, 8342, doi:10.1029/2001JD000626, 2002.

Baumgardner, D., Kok, G. L., and Raga, G. B.: On the diurnal variability of particle properties related to light absorbing carbon in Mexico City, Atmos. Chem. Phys., 7, 2517–2526, doi:10.5194/acp-7-2517-2007, 2007.

Bischoff-Gauß, I., Kalthoff, N., and Fiedler, F.: The impact of secondary flow systems on air pollution in the area of Sao Paulo, J. Appl. Meteorol., 37, 269–287, doi:10.1175/1520-0450-37.3.269, 1998.

Bond, T. C. and Bergstrom, R. W.: Light absorption by carbonaceous particles: An investigative review, Aerosol. Sci. Technol., 40, 27–67, doi:10.1080/02786820500421521, 2006.

CETESB: Relatório de Qualidade do Ar no Estado de São Paulo 2007: Série Relatórios, CETESB, São Paulo, SP, Brazil, ISSN 0103-4103, 2008.

Clarke, A. and Kapustin, V.: Hemispheric aerosol vertical profiles: Anthropogenic impacts on optical depth and cloud nuclei, Science, 329, 1488–1492, 2010.

Colon, M., Pleil, J. D., Hartlage, T. A., Guardani, M. L., and Martins, M. H.: Survey of volatile organic compounds associated with automative emissions in the urban airshed of Sao Paulo, Brazil, Atmos. Environ., 35, 4017–4031, 2001.

Compo, G. P., Whitaker, J. S., Sardeshmukh, P. D., Matsui, N., Allan, R. J., Yin, X., Gleason, B. E., Jr., Vose, R. S., Rutledge, G., Bessemoulin, P., Broennimann, S., Brunet, M., Crouthamel, R. I., Grant, A. N., Groisman, P. Y., Jones, P. D., Kruk, M. C., Kruger, A. C., Marshall, G. J., Maugeri, M., Mok, H. Y., Nordli, O., Ross, T. F., Trigo, R. M., Wang, X. L., Woodruff, S. D., and Worley, S. J.: The Twentieth Century Reanalysis Project, Q. J. Roy. Meteorol. Soc., 137, 1–28, doi:10.1002/qj.776, 2011.

Crutzen, P. and Zimmermann, P.: The Changing Photochemistry of the Troposphere, Tellus A, 43, 136–151, doi:10.1034/j.1600-0870.1991.00012.x, 1991.

Dal Maso, M., Kulmala, M., Lehtinen, K. E. J., Mäkelä, J. M., Aalto, P. P., and O'Dowd, C. D.: Condensation and coagulation sinks and formation of nucleation mode particles in coastal and boreal forest boundary layers, J. Geophys. Res.-Atmos., 107, 8097, doi:10.1029/2001JD001053, 2002.

Dal Maso, M., Kulmala, M., Riipinen, I., Wagner, R., Hussein, T., Aalto, P. P., and Lehtinen, K. E. J.: Formation and growth of fresh atmospheric aerosols: eight years of aerosol size distribution data from SMEAR II, Hyytiälä, Finland, Boreal Environ. Res., 10, 323–336, 2005.

Davidson, C., Phalen, R., and Solomon, P.: Airborne particulate matter and human health: A review, Aerosol. Sci. Technol., 39, 737–749, doi:10.1080/02786820500191348, 2005.

Dunn, M. J., Jimenez, J. L., Baumgardner, D., Castro, T., McMurry, P. H., and Smith, J. N.: Measurements of Mexico City nanoparticle size distributions: Observations of new particle formation and growth, Geophys. Res. Lett., 31, L10102, doi:10.1029/2004GL019483, 2004.

Estupinan, J., Raman, S., Crescenti, G., Streicher, J., and Barnard, W.: Effects of clouds and haze on UV-B radiation, J. Geophys. Res.-Atmos., 101, 16807–16816, doi:10.1029/96JD01170, 1996.

Farrell, A. E.: Ethanol can contribute to energy and environmental goals, Science, 311, 506–508, 2006.

Fuchs, N. A.: On the stationary charge distribution on aerosol particles in a bipolar ionic atmosphere, Pure Appl. Geophys., 56, 185–193, 1963.

Gaffney, J. S. and Marley, N. A.: The impacts of combustion emissions on air quality and climate – From coal to biofuels and beyond, Atmos. Environ., 43, 23–36, doi:10.1016/j.atmosenv.2008.09.016, 2009.

Gallardo, L., Escribano, J., Dawidowski, L., Rojas, N., Andrade, M. F., and Osses, M.: Evaluation of vehicle emission inventories for carbon monoxide and nitrogen oxides for Bogota, Buenos Aires, Santiago, and Sao Paulo, Atmos. Environ., 47, 12–19, doi:10.1016/j.atmosenv.2011.11.051, 2012.

Garland, R. M., Schmid, O., Nowak, A., Achtert, P., Wiedensohler, A., Gunthe, S. S., Takegawa, N., Kita, K., Kondo, Y., Hu, M., Shao, M., Zeng, L. M., Zhu, T., Andreae, M. O., and Pöschl, U.: Aerosol optical properties observed during Campaign of Air Quality Research in Beijing 2006 (CAREBeijing-2006): Characteristic differences between the inflow and out-

flow of Beijing city air, J. Geophys. Res.-Atmos., 114, D00G04, doi:10.1029/2008JD010780, 2009.

Graham, L. A., Belisle, S. L., and Baas, C.: Emissions from light duty gasoline vehicles operating on low blend ethanol gasoline and E85, Atmos. Environ., 42, 4498–4516, doi:10.1016/j.atmosenv.2008.01.061, 2008.

Gurjar, B. R., Butler, T. M., Lawrence, M. G., and Lelieveld, J.: Evaluation of emissions and air quality in megacities, Atmos. Environ., 42, 1593–1606, doi:10.1016/j.atmosenv.2007.10.048, 2008.

Haagen-Smit, A. J.: Chemistry and Physiology of Los-Angeles Smog, Industrial and Engineering Chemistry, 44, 1342–1346, 1952.

Hansen, J., Sato, M., and Ruedy, R.: Radiative forcing and climate response, J. Geophys. Res.-Atmos., 102, 6831–6864, 1997.

Hallquist, M., Wenger, J. C., Baltensperger, U., Rudich, Y., Simpson, D., Claeys, M., Dommen, J., Donahue, N. M., George, C., Goldstein, A. H., Hamilton, J. F., Herrmann, H., Hoffmann, T., Iinuma, Y., Jang, M., Jenkin, M. E., Jimenez, J. L., Kiendler-Scharr, A., Maenhaut, W., McFiggans, G., Mentel, Th. F., Monod, A., Prévôt, A. S. H., Seinfeld, J. H., Surratt, J. D., Szmigielski, R., and Wildt, J.: The formation, properties and impact of secondary organic aerosol: current and emerging issues, Atmos. Chem. Phys., 9, 5155–5236, doi:10.5194/acp-9-5155-2009, 2009.

Haywood, J. M. and Boucher, O.: Estimates of the direct and indirect radiative forcing due to tropospheric aerosols: A review, Rev. Geophys., 38, 513–543, 2000.

Haywood, J. and Shine, K.: The Effect of Anthropogenic Sulfate and Soot Aerosol on the Clear-Sky Planetary Radiation Budget, Geophys. Res. Lett., 22, 603–606, doi:10.1029/95GL00075, 1995.

Herrmann, P. and Hanel, G.: Wintertime optical properties of atmospheric particles and weather, Atmos. Environ., 31, 4053–4062, 1997.

Hirsikko, A., Laakso, L., Hõrrak, U., Aalto, P. P., Kerminen, V.-M., and Kulmala, M.: Annual and size dependent variation of growth rates and ion concentrations in boreal forest, Boreal Environ. Res., 10, 357–369, 2005.

Hussein, T., Dal Maso, M., Petäjä, T., Koponen, I. K., Paatero, P., Aalto, P. P., Hämeri, K., and Kulmala, M.: Evaluation of an automatic algorithm for fitting the particle number size distributions, Boreal Environ. Res., 10, 337–355, 2005.

Hyvärinen, A.-P., Lihavainen, H., Komppula, M., Sharma, V. P., Kerminen, V.-M., Panwar, T. S., and Viisanen, Y.: Continuous measurements of optical properties of atmospheric aerosols in Mukteshwar, northern India, J. Geophys. Res.-Atmos., 114, D08207, doi:10.1029/2008JD011489, 2009.

Hyvärinen, A.-P., Lihavainen, H., Komppula, M., Panwar, T. S., Sharma, V. P., Hooda, R. K., and Viisanen, Y.: Aerosol measurements at the Gual Pahari EUCAARI station: preliminary results from in-situ measurements, Atmos. Chem. Phys., 10, 7241–7252, doi:10.5194/acp-10-7241-2010, 2010.

IPCC: Climate Change 2007: The Physical Science Basis. Contribution of Working Group I to the Fourth Assessment Report of the Intergovernmental Panel on Climate Change, Cambridge University Press, Cambridge, United Kingdom and New York, NY, USA, 2007.

Jacob, D.: Heterogeneous chemistry and tropospheric ozone, Atmos. Environ., 34, 2131–2159, doi:10.1016/S1352-2310(99)00462-8, 2000.

Jacobson, M. Z.: Strong radiative heating due to the mixing state of black carbon in atmospheric aerosols, Nature, 409, 695–697, 2001.

Jacobson, M. Z.: Effects of ethanol (E85) versus gasoline vehicles on cancer and mortality in the United States, Environ. Sci. Technol., 41, 4150–4157, doi:10.1021/es062085v, 2007.

Jang, M. and Kamens, R. M.: Atmospheric Secondary Aerosol Formation by Heterogeneous Reactions of Aldehydes in the Presence of a Sulfuric Acid Aerosol Catalyst, Environ. Sci. Technol., 35, 4758–4766, doi:10.1021/es010790s, 2001.

Jenkin, M. and Clemitshaw, K.: Ozone and other secondary photochemical pollutants: chemical processes governing their formation in the planetary boundary layer, Atmos. Environ., 34, 2499–2527, doi:10.1016/S1352-2310(99)00478-1, 2000.

Jimenez, J. L., Canagaratna, M. R., Donahue, N. M., Prevot, A. S. H., Zhang, Q., Kroll, J. H., DeCarlo, P. F., Allan, J. D., Coe, H., Ng, N. L., Aiken, A. C., Docherty, K. S., Ulbrich, I. M., Grieshop, A. P., Robinson, A. L., Duplissy, J., Smith, J. D., Wilson, K. R., Lanz, V. A., Hueglin, C., Sun, Y. L., Tian, J., Laaksonen, A., Raatikainen, T., Rautiainen, J., Vaattovaara, P., Ehn, M., Kulmala, M., Tomlinson, J. M., Collins, D. R., Cubison, M. J., Dunlea, E. J., Huffman, J. A., Onasch, T. B., Alfarra, M. R., Williams, P. I., Bower, K., Kondo, Y., Schneider, J., Drewnick, F., Borrmann, S., Weimer, S., Demerjian, K., Salcedo, D., Cottrell, L., Griffin, R., Takami, A., Miyoshi, T., Hatakeyama, S., Shimono, A., Sun, J. Y., Zhang, Y. M., Dzepina, K., Kimmel, J. R., Sueper, D., Jayne, J. T., Herndon, S. C., Trimborn, A. M., Williams, L. R., Wood, E. C., Middlebrook, A. M., Kolb, C. E., Baltensperger, U., and Worsnop, D. R.: Evolution of Organic Aerosols in the Atmosphere, Science, 326, 1525–1529, doi:10.1126/science.1180353, 2009.

Kalafut-Pettibone, A. J., Wang, J., Eichinger, W. E., Clarke, A., Vay, S. A., Blake, D. R., and Stanier, C. O.: Size-resolved aerosol emission factors and new particle formation/growth activity occurring in Mexico City during the MILAGRO 2006 Campaign, Atmos. Chem. Phys., 11, 8861–8881, doi:10.5194/acp-11-8861-2011, 2011.

Kerminen, V.-M., Pirjola, L., and Kulmala, M.: How significantly does coagulational scavenging limit atmospheric particle production?, J. Geophys. Res.-Atmos., 106, 24119–24125, 2001.

Kerminen, V.-M., Lehtinen, K., Anttila, T., and Kulmala, M.: Dynamics of atmospheric nucleation mode particles: a timescale analysis, Tellus B, 56, 135–146, doi:10.1111/j.1600-0889.2004.00095.x, 2004.

Kittelson, D., Watts, W., and Johnson, J.: Nanoparticle emissions on Minnesota highways, Atmos. Environ., 38, 9–19, doi:10.1016/j.atmosenv.2003.09.037, 2004.

Knutson, E. O. and Whitby, K. T.: Aerosol classification by electric mobility: Apparatus, theory, and applications, J. Aerosol Sci., 6, 443–451, 1975.

Kroll, J. H. and Seinfeld, J. H.: Chemistry of secondary organic aerosol: Formation and evolution of low-volatility organics in the atmosphere, Atmos. Environ., 42, 3593–3624, doi:10.1016/j.atmosenv.2008.01.003, 2008.

Kulmala, M.: How particles nucleate and grow, Science, 302, 1000–1001, 2003.

Kulmala, M. and Tammet, H.: Finnish-Estonian air ion and aerosol workshops, Boreal Environ. Res., 12, 237–245, 2007.

Kulmala, M., Dal Maso, M., Mäkelä, J. M., Pirjola, L., Väkevä, M., Aalto, P. P., Miikkulainen, P., Hämeri, K., and O'Dowd, C. D.: On the formation, growth and composition of nucleation mode particles, Tellus B, 53, 479–490, 2001.

Kulmala, M., Vehkamäki, H., Petäjä, T., Dal Maso, M., Lauri, A., Kerminen, V.-M., Birmili, W., and McMurry, P. H.: Formation and growth rates of ultrafine atmospheric particles: a review of observations, J. Aerosol Sci., 35, 143–176, doi:10.1016/j.jaerosci.2003.10.003, 2004.

Kulmala, M., Petäjä, T., Mönkkönen, P., Koponen, I. K., Dal Maso, M., Aalto, P. P., Lehtinen, K. E. J., and Kerminen, V.-M.: On the growth of nucleation mode particles: source rates of condensable vapor in polluted and clean environments, Atmos. Chem. Phys., 5, 409–416, doi:10.5194/acp-5-409-2005, 2005.

Kulmala, M., Petäjä, T., Nieminen, T., Sipilä, M., Manninen, H. E., Lehtipalo, K., Dal Maso, M., Aalto, P. P., Junninen, H., Paasonen, P., Riipinen, I., Lehtinen, K. E. J., Laaksonen, A., and Kerminen, V.-M.: Measurement of the nucleation of atmospheric aerosol particles, Nat. Protocols, 7, 1651–1667, 2012.

Kusaka, H. and Kimura, F.: Coupling a single-layer urban canopy model with a simple atmospheric model: Impact on urban heat island simulation for an idealized case, J. Meteorol. Soc. Jpn., 82, 67–80, doi:10.2151/jmsj.82.67, 2004.

Laakso, L., Koponen, I. K., Mönkkönen, P., Kulmala, M., Kerminen, V.-M., Wehner, B., Wiedensohler, A., Wu, Z., and Hu, M.: Aerosol particles in the developing world; A comparison between New Delhi in India and Beijing in China, Water Air Soil Pollut., 173, 5–20, doi:10.1007/s11270-005-9018-5, 2006.

Lohmann, U. and Feichter, J.: Global indirect aerosol effects: a review, Atmos. Chem. Phys., 5, 715–737, doi:10.5194/acp-5-715-2005, 2005.

Manninen, H. E., Petäjä, T., Asmi, E., Riipinen, I., Nieminen, T., Mikkilä, J., Hõrrak, U., Mirme, A., Mirme, S., Laakso, L., Kerminen, V.-M., and Kulmala, M.: Long-term field measurements of charged and neutral clusters using Neutral cluster and Air Ion Spectrometer (NAIS), Boreal Environ. Res., 14, 591–605, 2009.

Meng, Z., Dabdub, D., and Seinfeld, J.: Chemical coupling between atmospheric ozone and particulate matter, Science, 277, 116–119, doi:10.1126/science.277.5322.116, 1997.

Mirme, S. and Mirme, A.: The mathematical principles and design of the NAIS – a spectrometer for the measurement of cluster ion and nanometer aerosol size distributions, Atmos. Meas. Tech. Discuss., 4, 7405–7434, doi:10.5194/amtd-4-7405-2011, 2011.

Mirme, A., Tamm, E., Mordas, G., Vana, M., Uin, J., Mirme, S., Bernotas, T., Laakso, L., Hirsikko, A., and Kulmala, M.: A wide-range multi-channel air ion spectrometer, Boreal Environ. Res., 12, 247–264, 2007.

Mönkkönen, P., Koponen, I. K., Lehtinen, K. E. J., Hämeri, K., Uma, R., and Kulmala, M.: Measurements in a highly polluted Asian mega city: observations of aerosol number size distribution, modal parameters and nucleation events, Atmos. Chem. Phys., 5, 57–66, doi:10.5194/acp-5-57-2005, 2005.

Müller, T., Henzing, J. S., de Leeuw, G., Wiedensohler, A., Alastuey, A., Angelov, H., Bizjak, M., Collaud Coen, M., Engström, J. E., Gruening, C., Hillamo, R., Hoffer, A., Imre, K., Ivanow, P., Jennings, G., Sun, J. Y., Kalivitis, N., Karlsson, H., Komppula, M., Laj, P., Li, S.-M., Lunder, C., Marinoni, A., Mar-

tins dos Santos, S., Moerman, M., Nowak, A., Ogren, J. A., Petzold, A., Pichon, J. M., Rodriquez, S., Sharma, S., Sheridan, P. J., Teinilä, K., Tuch, T., Viana, M., Virkkula, A., Weingartner, E., Wilhelm, R., and Wang, Y. Q.: Characterization and intercomparison of aerosol absorption photometers: result of two intercomparison workshops, Atmos. Meas. Tech., 4, 245–268, doi:10.5194/amt-4-245-2011, 2011.

Neitola, K., Asmi, E., Komppula, M., Hyvärinen, A.-P., Raatikainen, T., Panwar, T. S., Sharma, V. P., and Lihavainen, H.: New particle formation infrequently observed in Himalayan foothills – why?, Atmos. Chem. Phys., 11, 8447–8458, doi:10.5194/acp-11-8447-2011, 2011.

Nel, A.: Air pollution-related illness: Effects of particles, Science, 308, 804–806, doi:10.1126/science.1108752, 2005.

Nguyen, H. T., Takenaka, N., Bandow, H., Maeda, Y., de Oliva, S. T., Botelho, M. M. f., and Tavares, T. M.: Atmospheric alcohols and aldehydes concentrations measured in Osaka, Japan and in Sao Paulo, Brazil, Atmos. Environ., 35, 3075–3083, doi:10.1016/S1352-2310(01)00136-4, 2001.

Nieminen, T., Manninen, H. E., Sihto, S.-L., Yli-Juuti, T., Mauldin, R. L., Petäjä, T., Riipinen, I., Kerminen, V.-M., and Kulmala, M.: Connection of Sulfuric Acid to Atmospheric Nucleation in Boreal Forest, Environ. Sci. Technol., 43, 4715–4721, doi:10.1021/es803152j, 2009.

Nieminen, T., Lehtinen, K. E. J., and Kulmala, M.: Sub-10 nm particle growth by vapor condensation – effects of vapor molecule size and particle thermal speed, Atmos. Chem. Phys., 10, 9773–9779, doi:10.5194/acp-10-9773-2010, 2010.

Oke, T.: The Energetic Basis of the Urban Heat-Island, Q. J. Roy. Meteorol. Soc., 108, 1–24, doi:10.1002/qj.49710845502, 1982.

Oke, T.: The Urban Energy-Balance, Prog. Phys. Geogr., 12, 471–508, doi:10.1177/030913338801200401, 1988.

Oliveira, A. P., Machado, A. J., Escobedo, J. F., and Soares, J.: Diurnal evolution of solar radiation at the surface in the city of Sao Paulo: seasonal variation and modeling, Theor. Appl. Climatol., 71, 231–250, 2002.

Oliveira, A. P., Bornstein, R. D., and Soares, J.: Annual and Diurnal Wind Patterns in the City of São Paulo, Water Air Soil Pollut., 3, 3–15, 2003.

Orlando, J. P., Alvim, D. S., Yamazaki, A., Correa, S. M., and Gatti, L. V.: Ozone precursors for the Sao Paulo Metropolitan Area, Sci. Total Environ., 408, 1612–1620, doi:10.1016/j.scitotenv.2009.11.060, 2010.

Paredes-Miranda, G., Arnott, W. P., Jimenez, J. L., Aiken, A. C., Gaffney, J. S., and Marley, N. A.: Primary and secondary contributions to aerosol light scattering and absorption in Mexico City during the MILAGRO 2006 campaign, Atmos. Chem. Phys., 9, 3721–3730, doi:10.5194/acp-9-3721-2009, 2009.

Petzold, A., Schloesser, H., Sheridan, P. J., Arnott, W. P., Ogren, J. A., and Virkkula, A.: Evaluation of multiangle absorption photometry for measuring aerosol light absorption, Aerosol. Sci. Technol., 39, 40–51, doi:10.1080/027868290901945, 2005.

Petäjä, T., Mauldin, III, R. L., Kosciuch, E., McGrath, J., Nieminen, T., Paasonen, P., Boy, M., Adamov, A., Kotiaho, T., and Kulmala, M.: Sulfuric acid and OH concentrations in a boreal forest site, Atmos. Chem. Phys., 9, 7435–7448, doi:10.5194/acp-9-7435-2009, 2009.

Pöschl, U., Martin, S. T., Sinha, B., Chen, Q., Gunthe, S. S., Huffman, J. A., Borrmann, S., Farmer, D. K., Garland, R. M.,

Helas, G., Jimenez, J. L., King, S. M., Manzi, A., Mikhailov, E., Pauliquevis, T., Petters, M. D., Prenni, A. J., Roldin, P., Rose, D., Schneider, J., Su, H., Zorn, S. R., Artaxo, P., and Andreae, M. O.: Rainforest Aerosols as Biogenic Nuclei of Clouds and Precipitation in the Amazon, Science, 329, 1513–1516, doi:10.1126/science.1191056, 2010.

Ramanathan, V. and Carmichael, G.: Global and regional climate changes due to black carbon, Nat. Geosci., 1, 221–227, doi:10.1038/ngeo156, 2008.

Ramanathan, V., Crutzen, P. J., Kiehl, J. T., and Rosenfeld, D.: Atmosphere – Aerosols, climate, and the hydrological cycle, Science, 294, 2119–2124, 2001.

Rudich, Y., Donahue, N. M., and Mentel, T. F.: Aging of organic aerosol: Bridging the gap between laboratory and field studies, Annu. Rev. Phys. Chem., 58, 321–352, doi:10.1146/annurev.physchem.58.032806.104432, 2007.

Satheesh, S. K., Vinoj, V., and Moorthy, K. K.: Radiative effects of aerosols at an urban location in southern India: Observations versus model, Atmos. Environ., 44, 5295–5304, doi:10.1016/j.atmosenv.2010.07.020, 2010.

Schafer, J., Saxena, V., Wenny, B., Barnard, W., and DeLuisi, J.: Observed influence of clouds on ultraviolet-B radiation, Geophys. Res. Lett., 23, 2625–2628, doi:10.1029/96GL01984, 1996.

Seinfeld, J.: Urban Air-Pollution – State of the Science, Science, 243, 745–752, doi:10.1126/science.243.4892.745, 1989.

Silva Júnior, R. S., de Oliveira, M. G. L., and Andrade, M. F.: Weekend/weekday differences in concentrations of ozone, nox, and non-methane hydrocarbon in the metropolitan area of São Paulo, Revista Brasileira de Meteorologia, 24, 100–110, 2009.

Sipilä, M., Berndt, T., Petäjä, T., Brus, D., Vanhanen, J., Stratmann, F., Patokoski, J., Mauldin, R. L., Hyvärinen, A., Lihavainen, H., and Kulmala, M.: The Role of Sulfuric Acid in Atmospheric Nucleation, Science, 327, 1243–1246, doi:10.1126/science.1180315, 2010.

Sturm, P., Baltensperger, U., Bacher, M., Lechner, B., Hausberger, S., Heiden, B., Imhof, D., Weingartner, E., Prevot, A., Kurtenbach, R., and Wiesen, P.: Roadside measurements of particulate matter size distribution, Atmos. Environ., 37, 5273–5281, doi:10.1016/j.atmosenv.2003.05.006, 2003.

Tammet, H. and Kulmala, M.: Simulation tool for atmospheric aerosol nucleation bursts, J. Aerosol Sci., 36, 173–196, doi:10.1016/j.jaerosci.2004.08.004, 2005.

Tanner, R., Miguel, A., Deandrade, J., Gaffney, J., and Streit, G.: Atmospheric Chemistry of Aldehydes – Enhanced Peroxyacetyl Nitrate Formation from Ethanol-Fueled Vehicular Emissions, Environ. Sci. Technol., 22, 1026–1034, doi:10.1021/es00174a005, 1988.

Wehner, B., Birmili, W., Gnauk, T., and Wiedensohler, A.: Particle number size distributions in a street canyon and their transformation into the urban-air background: measurements and a simple model study, Atmos. Environ., 36, 2215–2223, doi:10.1016/S1352-2310(02)00174-7, 2002.

Wehner, B., Wiedensohler, A., Tuch, T. M., Wu, Z. J., Hu, M., Slanina, J., and Kiang, C. S.: Variability of the aerosol number size distribution in Beijing, China: New particle formation, dust storms, and high continental background, Geophys. Res. Lett., 31, L22108, doi:10.1029/2004GL021596, 2004.

Wehner, B., Petäjä, T., Boy, M., Engler, C., Birmili, W., Tuch, T., Wiedensohler, A., and Kulmala, M.: The contribution of sulfuric acid and non-volatile compounds on the growth of freshly formed atmospheric aerosols, Geophys. Res. Lett., 32, L17810, doi:10.1029/2005GL023827, 2005.

Winklmayr, W., Reischl, G. P., Lindner, A. O., and Berner, A.: A New Electromobility Spectrometer for the Measurement of Aerosol Size Distributions in the Size Range from 1 to 1000 Nm, J. Aerosol Sci., 22, 289–296, 1991.

Wu, Z., Hu, M., Liu, S., Wehner, B., Bauer, S., Ssling, A. M., Wiedensohler, A., Petäjä, T., Dal Maso, M. and Kulmala, M.: New particle formation in Beijing, China: Statistical analysis of a 1-year data set, J. Geophys. Res.-Atmos., 112, D09209, doi:10.1029/2006JD007406, 2007.

Yli-Juuti, T., Nieminen, T., Hirsikko, A., Aalto, P. P., Asmi, E., Hõrrak, U., Manninen, H. E., Patokoski, J., Dal Maso, M., Petäjä, T., Rinne, J., Kulmala, M., and Riipinen, I.: Growth rates of nucleation mode particles in Hyytiälä during 2003–2009: variation with particle size, season, data analysis method and ambient conditions, Atmos. Chem. Phys., 11, 12865–12886, doi:10.5194/acp-11-12865-2011, 2011.

Zhang, R.: Getting to the Critical Nucleus of Aerosol Formation, Science, 328, 1366–1367, doi:10.1126/science.1189732, 2010.

Zhang, S. H. and Flagan, R. C.: Resolution of the radial differential mobility analyzer for ultrafine particles, J. Aerosol Sci., 27, 1179–1200, 1996.

Zhang, Y., Seigneur, C., Seinfeld, J. H., Jacobson, M., Clegg, S. L., and Binkowski, F. S.: A comparative review of inorganic aerosol thermodynamic equilibrium modules: similarities, differences, and their likely causes, Atmos. Environ., 34, 117–137, doi:10.1016/S1352-2310(99)00236-8, 2000.

Zhu, Y., Hinds, W., Kim, S., Shen, S., and Sioutas, C.: Study of ultrafine particles near a major highway with heavy-duty diesel traffic, Atmos. Environ., 36, 4323–4335, 10.1016/S1352-2310(02)00354-0, 2002.